Vesa Koiramäki

Development of printable membrane electrode assembly for a passive direct methanol fuel cell-based biosensor

Helsinki Metropolia University of Applied Sciences

Bachelor of Engineering

Biotechnology and Food Engineering

Bachelor's Thesis

30 August 2016

Metropolia

Author Title Number of Pages Date	Vesa Koiramäki Development of printable membrane electrode assembly for a passive direct methanol fuel cell-based biosensor 58 pages + 6 appendices 30 August 2016
Degree	Bachelor of Engineering
Degree Programme	Biotechnology and Food Engineering
Specialisation option	Biomedicine
Instructors	Saara Tuurala, Senior Scientist Pentti Viluksela, Principal Lecturer

This bachelor's thesis was carried out in co-operation with VTT at Micronova (Centre for Micro and Nanotechnology) in Dr Maria Smolander's research team (printed sensors and electronic devices) as part of the European Union co-funded Symbiotic project under the Future and Emerging Technologies (FET) programme.

Biosensors are important tools for recognising specific biomarkers that can be used to determine a person's state of health. A common problem is that amperometric biosensors require electricity and therefore their use is limited by the proximity of an electricity generator system. In-situ-constructed printable direct methanol fuel cell offers a compact power source for such applications.

The aim of this work was to develop and build prototype membrane electrode assembly for a passive air-breathing direct methanol fuel cell by using inkjet printing technology. Additionally, the methanol oxidation catalysis activity of the ink (Pt-Ru/C) used in production was verified.

The catalysis activity of the production ink was investigated in cyclic voltammetry by comparing it to inactive carbon black (Vulcan XC-72R) ink in both active and inactive electrolyte solution. The direct methanol fuel cell membrane electrode assembly prototype was constructed using Pt-Ru/C ink.

The results obtained support the methanol oxidation catalysis activity of the Pt-Ru/C ink and its potential usage in inkjet printing for direct methanol membrane electrode assembly construction. However, more research is still needed in membrane electrode assembly construction.

Keywords	membrane electrode assembly, passive direct methanol fuel cell, biosensor

Tekijä Otsikko Sivumäärä Aika	Vesa Koiramäki Tulostettavan passiivisen metanolipolttokennon membraani-elektrodikokoonpanon kehitys biosensoriin 58 sivua + 6 liitettä 30.8.2016
Tutkinto	Insinööri (AMK)
Koulutusohjelma	Bio- ja elintarviketekniikka
Suuntautumisvaihtoehto	Biolääketiede
Ohjaajat	Vanhempi tutkija Saara Tuurala Yliopettaja Pentti Viluksela

Opinnäytetyö toteutettiin yhteistyössä mikro- ja nanotekniikan keskuksen kanssa tri Maria Smolanderin tutkimusryhmässä osana Euroopan Unionin FET-ohjelman rahoittamaa Symbiotic-projektia. Symbiotic-projektin lopputavoitteena on kehittää täysin omavarainen sähkökemiallinen biosensori.

Biosensorit ovat tärkeitä diagnostisia työvälineitä tunnistamaan spesifisiä biomerkkiaineita, joita voidaan käyttää henkilön terveydentilan arviointiin. Yleinen ongelma on kuitenkin, että amperometriset biosensorit vaativat sähköä toimiakseen ja siten niiden käyttöetäisyys on rajattu sähkögeneraattorin läheisyyteen. Biosensoriin paikallisesti asennettava tulostettava metanolipolttokenno mahdollistaa kompaktin sähkönlähteen tällaisiin sovellutuksiin.

Opinnäytetyön aiheena oli tulostustekniikkaa hyödyntävän membraani-elektrodikokoonpanoprototyypin kehittäminen ja rakentaminen ilmahengitteiseen suoratoimiseen metanolipolttokennoon. Lisäksi katalyyttikerroksen valmistuksessa käytettävän platina-ruthenium-hiilimusteen (Pt-Ru/C) sopivuuden varmistaminen tulostettavan metanolipolttokennon anodikatalyytiksi.

Musteen katalyysiaktiivisuutta tutkittiin syklisellä voltammetrialla vertaamalla musteen aktiivisuutta puhtaasta hiilimustasta (Vulcan XC-72R) valmistettuun musteeseen sekä aktiivisessa että ei-aktiivisessa elektrolyytissä. Myös suora metanolipolttokennoprototyyppi rakennettiin käyttäen Pt-Ru/C-pohjaista mustetta.

Tulokset tukevat valmistetun musteen sopivuutta passiivin metanolimembraanielektrodikokoonpanon valmistamiseen, toisaalta lisätutkimusta vaaditaan tulostuskomponenttien yhteen liittämiseen kokoonpanossa.

Avainsanat	membraani-elektrodikokoonpano, passiivi suora metanolipolttokenno, biosensori

Preface

I am most grateful to Dr Maria Smolander for the opportunity to write my bachelor's thesis in her team at the Centre of Micro and Nanotechnology (VTT Technical Research Centre of Finland).

I want to express my deepest appreciation to my instructor Saara Tuurala for all the help and support, direct feedback, trust and freedom.

I am also extremely thankful to Pirjo Hakkarainen for showing me the laboratories and helping me to use devices and techniques needed in my final project and sharing her expertise related to this project. Additionally, I want to thank Kim Eiroma for explaining brief theory behind the functional materials inkjet printing and Anu Vaari for all the help in the design of experiments.

Finally, I want to thank everyone in team for their excellent support and showing the enthusiasm to my and their own work. I also want to thank my thesis instructor Dr Pentti Viluksela for all the support and trust he showed to me when I worked with my thesis in this project.

This all contributed to the atmosphere that was most exciting and enthusiastic, yet pleasantly tranquil, experience to focus on and work in. Thank you all. ☺

Helsinki 30.08.2016

Vesa Koiramäki

Contents

Nomenclature

Symbol	Description	Value / unit
A	Area	m^2
a	Thermodynamic activity	
E	Electrode potential	V
e	Elementary charge	1.6022×10^{-19} C
F	Faraday constant	96485 C mol^{-1}
G	Gibbs free energy	J
H	Entalphy	J
I	Electric current	A
m	Mass	kg
N_A	Avogadro constant	6.0221×10^{23} mol^{-1}
n	Amount of substance in moles	mol
Q	Reaction quotient	
R	Gas constant	8.3145 m^3 Pa K^{-1} mol^{-1}
T	Temperature	K
t	Time	s
U	Electric potential difference	V
V	Volume	m^3
Δ	Change in something	
η	Efficiency	
ν	Stoichiometric coefficient	
ρ	Density	kg m^{-3}

Abbreviations

AC	Alternating current
AFC	Alkaline fuel cell
BFC	Biological fuel cell
CMP	Carbon monoxide poisoning
CNT	Carbon nanotube
CV	Cyclic voltammetry
DAA	Diacetone alcohol
DC	Direct current
DET	Direct electron transfer
DIW	Deionised water
DMFC	Direct methanol fuel cell
GDL	Gas diffusion layer
IJP	Inkjet printing
MEA	Membrane electrode assembly
MET	Mediated electron transfer
MeOH	Methanol
MIP	Molecularly imprinted polymer
MPL	Microporous layer
OCV	Open-circuit voltage
PAFC	Phosphoric acid fuel cell
PEMFC	Proton exchange membrane fuel cell
PET	Polyethylene terephthalate
PTFE	Polytetrafluoroethylene
RHE	Reversible hydrogen electrode
SATP	Standard ambient temperature and pressure (298.15 K, 100 kPa)
SHE	Standard hydrogen electrode
SOFC	Solid oxide fuel cell
SPAM	Smart plastic antibody material
STP	Standard temperature and pressure (273.15 K, 100 kPa)
YSZ	Yttria-stabilized zirconia
Å	Ångström (0.1 nm)
mil	Thousandth of an inch (25.4 µm)
ppm	Parts per million

Subscripts

Chem	Chemical
Elec	Electrical
Ox	Oxidation
Reag	Reagent
Red	Reduction
Redox	Reduction-oxidation
Rxn	Reaction
Prod	Product

(aq)	Aqueous
(g)	Gas
(l)	Liquid
(s)	Solid

1 Introduction

This Bachelor's thesis was carried out in co-operation with VTT at Micronova (Centre for Micro and Nanotechnology) in Dr Maria Smolander's research team (printed sensors and electronic devices) as part of the European Union co-funded Symbiotic project under the Future and Emerging Technologies (FET) programme.

Symbiotic is an intereuropean European Union co-funded project between the Imperial College London (The Imperial College of Science, Technology and Medicine), UNINOVA (Institute for the Development of New Technologies), Aarhus University, Instituto Superior de Engenharia do Porto (Polytechnic of Porto - School of Engineering) and VTT (Technical Research Centre of Finland Ltd). The name Symbiotic is for "innovative autonomous electrical biosensor synergistically assembled inside a passive direct methanol fuel cell for screening cancer biomarkers". [1]

The intention of the Symbiotic project is to develop an autonomous electrochemical biosensor that is lightweight, disposable and low cost. As part of the project VTT is developing low cost, disposable fuel cells using printable technology on passive DMFC development for the Symbiotic biosensor. [2]

Cancer is a general term for describing a group of diseases that leads to abnormal cell growth in affected cells, i.e. cancer cells. Generally, cancer cells will keep proliferating and redistributing these cancer properties and, in some cases, forming tumours. The type of cancer and how it is located, e.g. accessibility to blood circulatory system, will determine if the cancer cells will stay benignly local or malignantly spread to the other parts of the body. The rate of cancer being able to spread new cancer cells is directly proportional to the number of viable cancer cells and thus also to time.

Biosensors are important tools for recognising specific biomolecules such as biomarkers, which can be used to determine a person's state of health. Amperometric biosensors can detect specific bioanalytes by converting biological entity (e.g. protein, nucleic acids and metabolic compounds) into an electrical signal that can be detected and analysed. The measurable changes in electrical properties of bio-recognition element enables making biosensors that can have high specificity and sensitivity, which holds vast potential for early disease detection and treatment. [3]

A common problem is that amperometric biosensors require electricity and therefore their use is limited by the proximity of an electricity generator system. Electricity is movement of electrons in electric gradient between the two sources of different electric potential energy. In daily life, the null potential is often referred as ground.

Classically, electricity is generated from fuels through a process which involves four conversion steps. First, the fuel is combusted that converts chemical energy into heat and produces exhaust gas. The heat is then used to boil water to make steam. The steam provides mechanical energy that runs a steam turbine. Finally, the mechanical energy turns into electricity in a running electric generator.[4]

A fuel cell, conversely, skips all these required steps and generates electricity in a one single step without any mechanical parts. The concept and scientific fundamentals for a fuel cell have existed over the past one and a half century, meaning that the fuel cell concept is actually older than the starting point of modern petroleum industry[5]. Still, only the last half of a century has actually seen the real practical utilisation of fuel cells. Now the trend has changed; new technologies are being developed and matured. The interest for the fuel cells is also strongly increasing due to the efficiency, environmental concerns and the decrease in fossil fuel resources. [4,6]

Inkjet printing technology offers the ability to accurately and in a controlled manner print a fixed amount of functional materials, such as catalysis layer of direct methanol fuel cell. This can help to reduce the overall costs of a disposable methanol fuel cell as the usage of expensive materials, such as platinum, can be reduced to minimum level.

The theory part of this thesis serves as an introduction to the diverse world of fuel cells. In the experimental part, the activity of catalysis properties of prepared Pt-Ru/C ink is investigated using cyclic voltammetry. Finally, a primitive prototype of PEM-based direct methanol fuel cell with five MEAs is constructed using Pt-Ru/C inkjet-printed components and tested.

2 Theory

2.1 Symbiotic biosensor

Symbiotic is a project for developing a low-cost autonomous electrochemical biosensor for cancer screening (See Figure 1). The electricity is generated in situ by an integrated direct methanol fuel cell (DMFC) system. Methanol offers good energy density in liquid form for compact and portable devices that can be operated at ambient temperature.

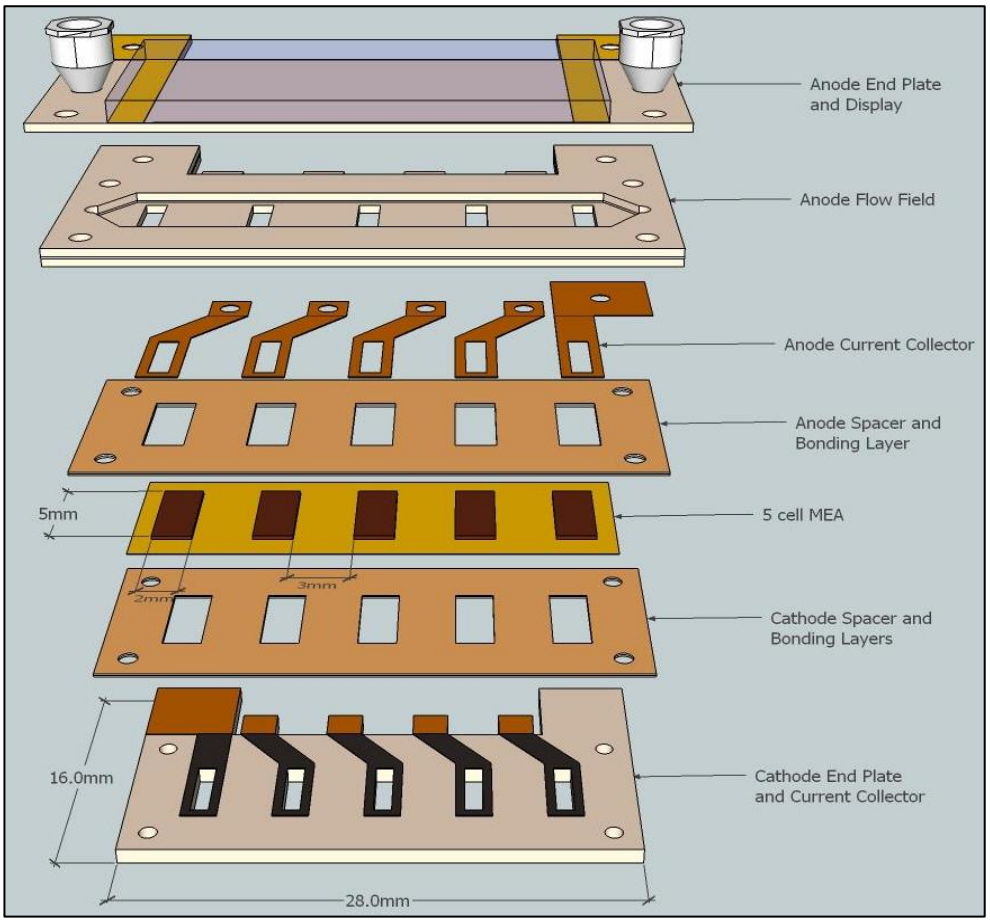

Figure 1. Concept (version 0.1 by Imperial College) stack design of Symbiotic biosensor

The main idea behind the concept is to incorporate an economical plastic bio-recognition element inside polymer membrane. The biosensor element with molecularly imprinted polymers (MIPs) is fixed to the anode of a passive DMFC. MIPs can be made sensitive to specific cancer biomarkers, thus activated by the presence of these bi-omarkers resulting change in the material's electrical properties that can be then measured. Generally, MIPs are more or less synthesised counterparts of biological

antibodies and they are commonly referred as plastic antibodies. Fairly new and interesting MIP synthesis technique is SPAM (see chapter 2.2).

Aqueous methanol is passively fed to the fuel cell anode and oxygen is provided from the air to the cathode for generating electricity to the biosensor system. Finally, this will result electrical current that is directly related to the resistance of MIP material that is related to the concentration of bound cancer biomarkers. This can be presented as a result. [7]

2.2 Smart plastic antibody material (SPAM)

Molecularly imprinted polymers (MIPs) are synthesised on top of an imprint target material. The imprinted molecule is then removed leaving a cavity in the MIP material. The cavity can then bind a new target molecule.

Generally, MIPs offer an inexpensive alternative to antibody-based immunoassays for recognising specific molecules by their active binding site. A target molecule that binds to the cavity will change some measurable property (e.g. conductivity) in MIP; therefore, the total concentration of target molecules can be evaluated by the overall total change in the measured property. Plastic antibodies are environmentally stable and specific for simple molecules [8]. Although MIPs work fairly well with small molecules, there are some issues with larger and more complex molecules; for instance, the specificity is often subpar compared to authentic biological protein antibodies.

SPAM is a new and promising synthesis technique for MIPs offering more specific binding to larger molecules. Synthesis of SPAM[9] is a five-step process that is presented in Figure 2. [9]

A layer of carboxylic acid (part A) is first activated. Then a template (e.g. protein) is allowed to attach to the surface (part B) of the activated carboxylic layer. The layer will bind with the biomolecule, in this example with functional carboxylic acid forming an amide bond with the protein.

Next, the electrically charged functional monomers are introduced (part C), in this case AMPSA with negative sulfonic acid group and AEMA with positive amine group. How-

ever, they are not completely in ionized form because the physiological conditions have to be ensured. If the physiological conditions are not met, the compatibility of the imprint for physiologically active molecule conformation cannot be guaranteed [10]. The unbound monomers are then washed. The unbound charged monomers could be problematic by replacing the neutral monomers in final polymerization, thus reducing the imprint specificity.

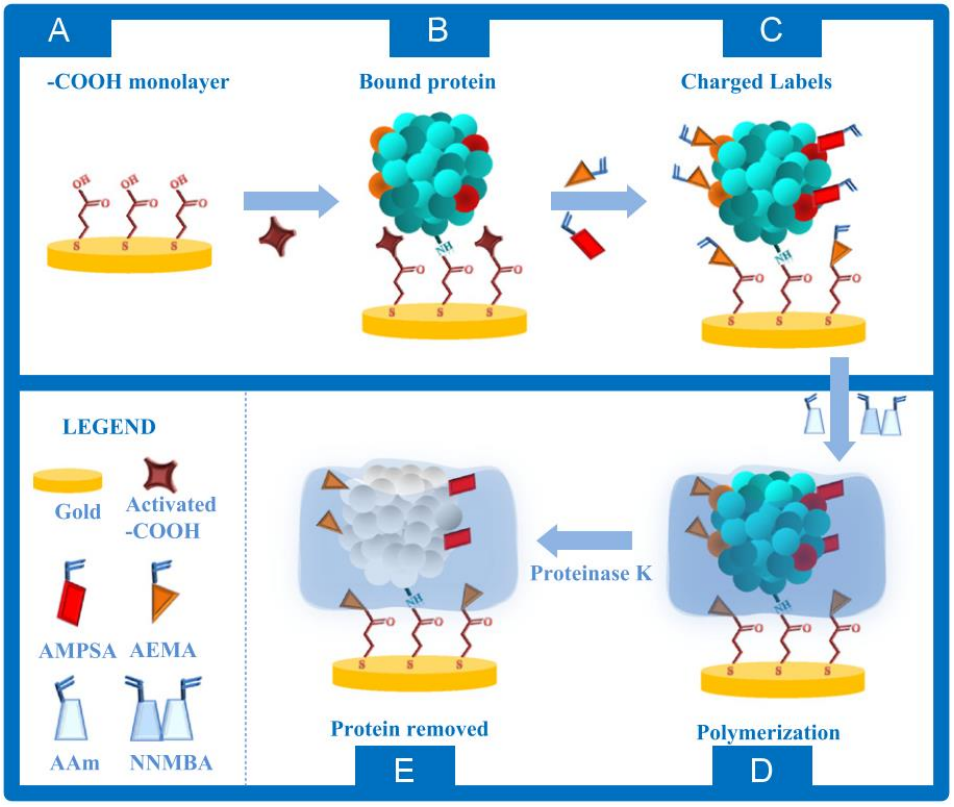

Figure 2. Schematic[9] for the synthetize of SPAM binding to myoglobin.

In the final polymerization (part D), the bound monomers are polymerized using neutral monomers. This will leave the imprint cavity for a biomolecule in the polymerized frame with specifically located functional groups. Finally, the imprint molecule (e.g. protein) is removed by clipping (e.g. utilising protease) it into smaller molecules and finally washing them away (part E). After washing, SPAM is ready to be collected.

2.3 Introduction to electricity and fuel cells

There are four generally accepted fundamental interactions that are supported by the evidence found in studies of nature and universe: gravity between masses (i), weak

interactions between elementary particles (ii), electromagnetic interactions between electrically charged particles (iii) and strong interactions between colour charges in atomic nuclei (iv). Table 1[11] presents the magnitudes of strength relative to the gravity interaction, other estimates exist[12].

Table 1. Strengths of fundamental interactions (according to W. Greiner and B. Müller) are presented relatively to the strength of gravity.

Interaction	Relative strength	Range (fm)
Gravitational interaction	1	Infinite
Weak nuclear interaction	10^{25}	$\ll 1$
Electromagnetic interaction	10^{38}	Infinite
Strong nuclear interaction	10^{41}	≈ 1

Every single atom has at least one proton. If the number of electrons in an atomic unit is greater than the number of protons the atom is called an anion, whereas if the number of electrons is less than the number of protons, it is then called a positively charged atom or a cation. The atom is said to be neutral if the count is same for electrons and protons. The opposite charges attract and the similar charges repel each other. The same principles are applied to polyatomic molecules.

Material's tendency to be reduced or oxidised, i.e. to acquire or release electron, is measured in reduction-oxidation (redox) potential, respectively. An electric current is produced by the movement of electrons in a conductive material between the two electrodes that have a different electrical potential, generating potential gradient between them. In DC electricity electrons move between two electrodes from the more negative anode to the more positive charged cathode. Alternatively, in AC electricity the direction of charged particles is reversed at constant intervals (e.g. 50 Hz) by switching the cathode and anode at the terminal ends.

Electric current travels via the path of least resistance through electric potential gradient. The movement of electrons is always less restricted than the movement of protons due to the electrons multitudes smaller mass. For this reason, electrons work as charge carriers in electricity [13]. Static electricity is asymmetry of charge in a matter, e.g. excess of electrons. A discharge of static electricity can be seen in a lightning phenomenon.

Materials known as insulators resist more the movement of charged particles and other materials correspondingly known as conductors allow more efficient movement of charged particles. Excluding superconductors, every material is a resistor to some degree.

Fuel cell transfers chemical energy into electrical energy, but some of this energy is lost as energy changes into a partially irreversible form of energy, e.g. heat (Equation 2.3.1), where E_{elec} is electrical energy, E_{chem} is chemical energy and E_{loss} is energy loss. Gibbs energy (Equation 2.3.2) is the maximum available work that can be performed by the reaction, where ΔH is change in enthalpy, T is temperature and ΔS change in entropy. The electrical energy equals to the change in Gibbs energy (ΔG) of reaction (Equation 2.3.3), where I is current, U electrical potential difference and t time. However it should be noted that it is theoretically applied to reversible fuel cells [14].

$$E_{elec} = E_{chem} - E_{loss} \tag{2.3.1}$$

$$\Delta G = \Delta H - T \times \Delta S \tag{2.3.2}$$

$$\Delta G_{rxn} = I \times U \times t - E_{loss} \tag{2.3.3}$$

$$\lim_{t \to 0}(U \times I \times t - E_{loss}) = U \times n_{electron} \times F \tag{2.3.4}$$

As time and therefore the number of electrons transferred approaches null, energy is not lost due to resistance and energy losses approaches null as well (Equation 2.3.4). In the equation $n_{electron}$ is moles of electrons transferred per mole of reactant and F is Faraday constant (charge per mole of electrons). This is referred as open-circuit voltage (OCV).

Assuming that the fuel cell is reversible and that, therefore all reaction energy is conserved and no energy is lost in electron transfer, the ideal voltage potential is approximately 1.2 V for a hydrogen fuel cell operating at standard ambient temperature and temperature (SATP) (Equation 2.3.7), where $E°$ is standard electrode potential. See Appendix 1 for formation energies and Appendix 5 for calculus details.

$$2\,H_2\,(g) + O_2(g) \longrightarrow 2\,H_2O\,(l) \tag{2.3.5}$$

$$\Delta G_{rxn} = \sum_{prod}(\nu_{\mathrm{prod}} \times \Delta \mathrm{G}_{\mathrm{prod,f}}^{\circ}) - \sum_{reag}(\nu_{\mathrm{reag}} \times \Delta \mathrm{G}_{\mathrm{reag,f}}^{\circ}) \tag{2.3.6}$$

$$E^{\circ} = \frac{\Delta G_{rxn}}{n_{electron} \times F} \tag{2.3.7}$$

Efficiency (Equation 2.3.7) of a fuel cell can be compared to the energy released if the fuel is burned, i.e. change in enthalpy of formation (Equation 2.3.6), where *v* is stoichiometric constant and ΔH_f° is standard heat of formation. This can be referred to either higher heating value (HHV) or lower heating value (LHV) depending the final state (liquid or gas) of water end-product. Although in practice not all fuel is reacted, a fuel utilisation coefficient (μ_f) can be used.

$$\Delta H_{rxn} = \sum_{prod}(\nu_{\mathrm{prod}} \times \Delta \mathrm{H}_{\mathrm{prod,f}}^{\circ}) - \sum_{reag}(\nu_{\mathrm{reag}} \times \Delta \mathrm{H}_{\mathrm{reag,f}}^{\circ}) \tag{2.3.6}$$

$$\eta = \mu_f \times \frac{\Delta G_{rxn}}{\Delta H_{rxn}} \tag{2.3.7}$$

Additionally, it should be clearly clarified that hardly any fuel cell has an environment that support constant temperature and pressure, therefore, Nernst equation (Equation 2.3.9) is often used to predict ideal potential more precisely, where *R* is gas constant and Q_{redox} is reaction quotient for reduction-oxidation reaction (Equation 2.3.8), where *a* is thermodynamic activity. [14]

$$Q_{redox} = \frac{\prod_{red}\left(a_{red}^{\nu_{red}}\right)}{\prod_{ox}(a_{ox}^{\nu_{ox}})} = \frac{[reduction\ activity]}{[oxidation\ activity]} \tag{2.3.8}$$

$$E_{cell} = E^{\circ} - \frac{R \times T}{n_{electron} \times F} \ln Q_{redox} \tag{2.3.9}$$

2.4 Cyclic voltammetry (CV)

Cyclic voltammetry is a technique that has become popular tool since the 1970s to obtain information about electron transfer processes. For instance, it can be used to study reaction pathways in biosynthesis or generation of free radicals in electrochemical reactions. [15]

The reaction of interest occurs on the working electrode. An auxiliary electrode (platinum) serves as a source or a sink for electrons. The potentials of other electrodes are measured against constant potential provided by a reference electrode (e.g. Ag/AgCl). [16]

In CV, current is measured as a function of voltage. Voltage is applied to the investigated working (testing) electrode that is scanned by changing voltages by scan rate (E_{step}/τ, where E_{step} is absolute value of voltage change and τ is interval) from the initial value (E_i) to the limit voltage value ($E_{\lambda 1}$). At the limit value the scan is reversed, and it is scanned to the other limit voltage value ($E_{\lambda 2}$). The cathodic (reduction) peak can be seen at +0.1 V and the anodic (oxidation) peak at +0.2 V in the example voltammogram, see Figure 3.

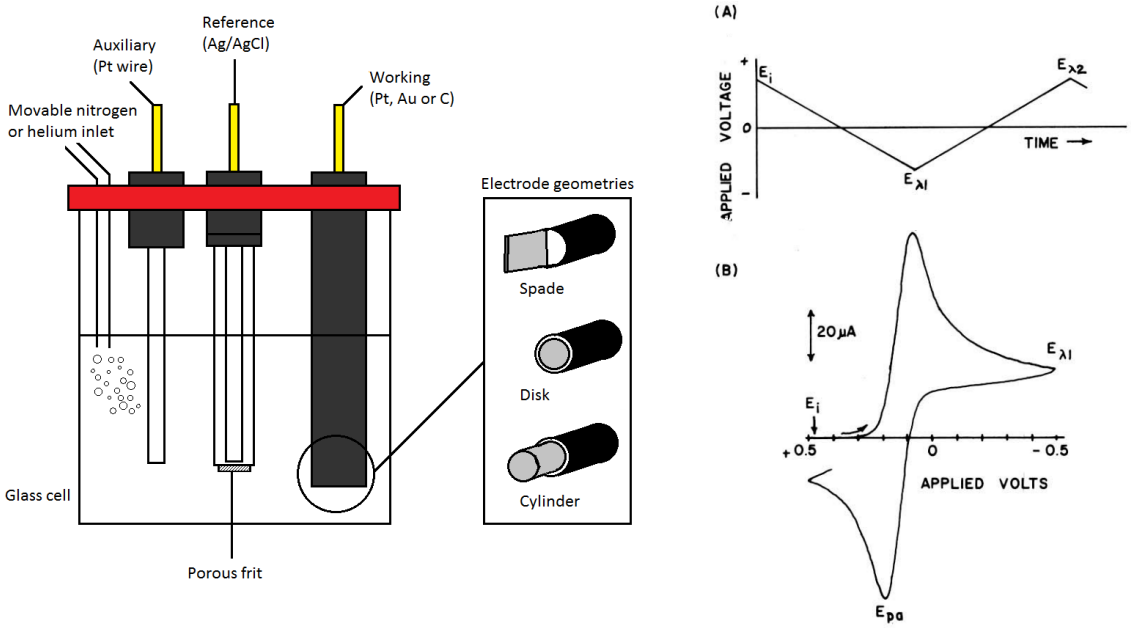

Figure 3. Illustration of typical setup in cyclic voltammetry is presented at left. Applied potential program (A) showing the potential limits $E_{\lambda 1}$ and $E_{\lambda 2}$ and an example of typical cyclic voltammogram (B) [15].

For successful electron transfer kinetics, it is essential that the surface of working electrode is polished and cleaned. Attention should also be paid to the choice of materials in the working electrode, for instance carbon electrodes are useful for detecting reactions of oxidation[17]. In some cases, especially when working with carbon electrodes,

it is advocated that the electrode surface should be activated by applying sequences of extreme positive and negative potentials. [15]

Depending on measurement environment the peak potentials in voltammograms may be affected by changes in pH that can directly contribute to electron-proton transfer reaction mechanisms[17].

2.5 Fuel cell technologies

Fuel cell is a device or a unit that converts chemical energy into DC electricity and produces heat and by-products such as water. In a minimalistic structure, a fuel cell consists of an intermediate electrolyte membrane with the two electrode layers on the opposite planes, i.e. electrolyte is technically sandwiched between the anode and the cathode (see Figure 4). Analogously it is quite similar to a battery, but, unlike a battery, a fuel cell produces waste by-products and heat. The electricity is generated directly from the oxidation of fuel, e.g. hydrogen through redox reaction. [6]

Additionally, there are different types of biological fuel cells which may be based on either direct enzymatic activity or more complex microbiological activities. These are still mostly at concept level but under moderately active research. New innovative fuel cells are compelling because various types of current fuel cell generation utilise expensive platinum-based catalyst materials. [18]

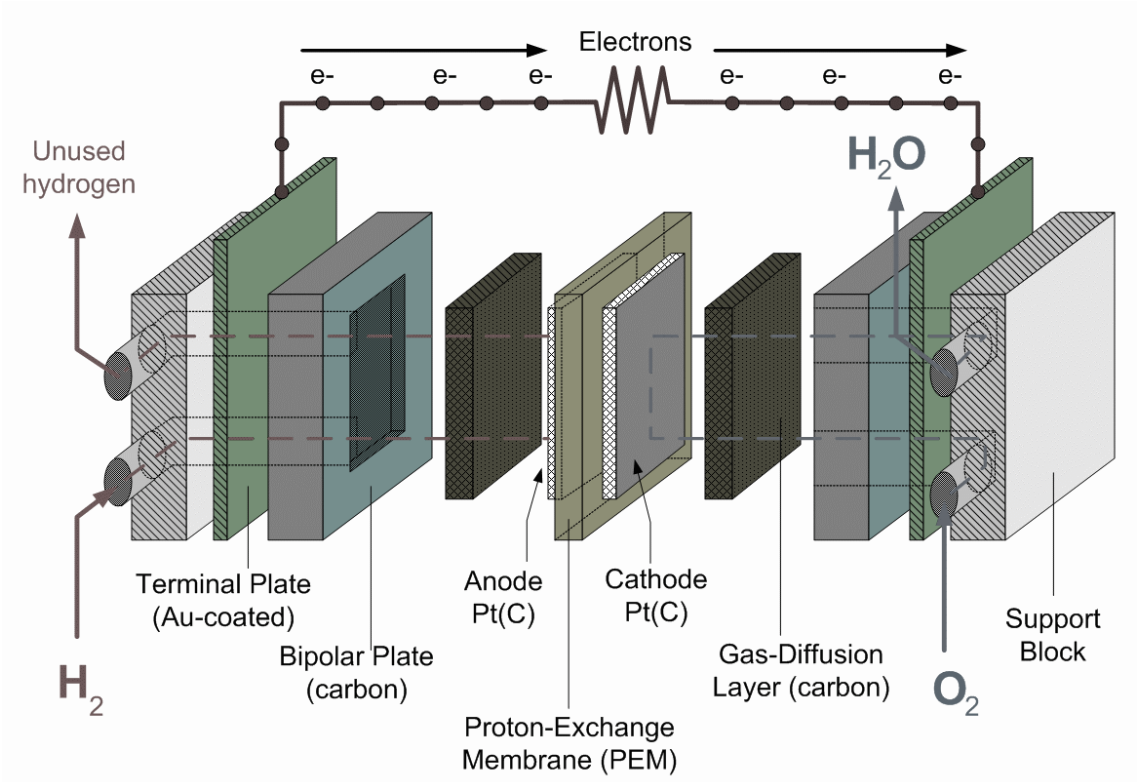

Figure 4. Presentation of the PEMFC structure by M. Fedkin[19]. Hydrogen circulates anode and oxygen circulates cathode. The catalyst layers are presented in this picture as an integral part of electrodes, catalyst layer is located at the interface of electrode and electrolyte (PEM).

Fuel cell technologies can primarily be classified (see Table 2) into major categories by the kind of electrolyte the cells utilise. These main categories include inter alia alkaline fuel cell (AFC), proton exchange membrane fuel cell (PEMFC), phosphoric acid fuel cell (PAFC), molten carbon fuel cell (MCFC) and solid oxide fuel cell (SOFC). Alternatively, fuel cells can be classified by the type of fuel consumed. For example, direct methanol fuel cell (DMFC) that oxidises directly methanol. DMFC is often PEM-based hence PEMDMFC or sometimes DM-PEMFC[20].

Fuel cell can be active or passive. In a passive fuel cell, no external force is applied to supply the fuel and oxygen to the cell. It is completely fed by using internal forces such as gravity, diffusion et cetera and combination of them, e.g. capillary action through wick[21] utilising adhesion and cohesion. In an active fuel cell, a pump can be used instead.

Table 2. Different fuel cell types listed with typical properties according to O. Sharaf and M. Orhan[6].

Type	Electrolyte	Anode	Cathode	Conduction	Fuel	Charge carrier	Power density	Efficiency (%)	Contaminants
PEMFC	Solid Nafion	Platinum, carbon support	Platinum, carbon support	Graphite	Hydrogen	Proton	High	40 – 60	Carbon monoxide, hydrogen sulphide
AFC	Potassium hydroxide, liquid solution	Nickel	Silver, carbon support	Graphite	Hydrogen	Hydroxide	Low	60 – 70	Carbon dioxide
PAFC	Phosphoric acid	Platinum, carbon support	Platinum, carbon support	Graphite	Hydrogen	Proton	Low	40	Carbon monoxide, siloxane, hydrogen sulphide
MCFC	Liquid alkali carbonate	Nickel chromium	Lithiated nickel oxide	Stainless steel	Methane	Carbonate	Low	Above 50	Sulphides, halides
SOFC	Solid yttria-stabilized zirconia	Nickel-YSZ composite	Strontium-doped lanthanum manganite	Ceramics	Methane	Oxide ion	Low	Above 50	Sulphides
DMFC	Solid polymer membrane	Platinum-Ruthenium, carbon support	Platinum, carbon support	Graphite	Methanol	Proton	Low	35 – 60	Carbon monoxide
Microbial	Ion exchange membrane	Biocatalyst, carbon support	Platinum, carbon support	N/A	Organic (e.g. glucose, biowaste)	Proton	Very low	15 – 65	Microbial contamination
Enzymatic	No membrane / Ion exchange membrane	Biocatalyst, carbon support	Biocatalyst, carbon support	N/A	Organic (e.g. glucose)	Proton	Low	30	External physical or chemical exposure

Some predictions expect that in the current century fuel cells will be replacing the conventional heat engines. Since fuel cells are not heat engines, their efficiency is not subjectable to the theoretical limitations defined by the Carnot cycle. Also electrochemical properties in fuel cells make them very interesting and applicable to many different problems found in today's electricity-dependent world. Fuel cells can be scaled from powering milliwatts to a microscale biosensor to hundreds of kilowatts to a full-scale industrial setting [22]. [4,6]

2.5.1 Proton exchange membrane fuel cell (PEMFC)

PEMFCs utilise a proton exchange membrane (PEM) that is ideally conductive to protons (proton exchange) but impermeable to gases and electrons. The PEM is sandwiched between two electrodes; an anode and a cathode.

The electrodes gas diffusion layer (GDL) is porous material that allows free flow for molecules. It is commonly made of carbon fabric. Additionally, there is a catalyst layer often with platinum particles at the interface between the electrode and the sandwiched membrane [4]. The catalyst layer is considered part of electrode layer. See Figure 5 for schematics.

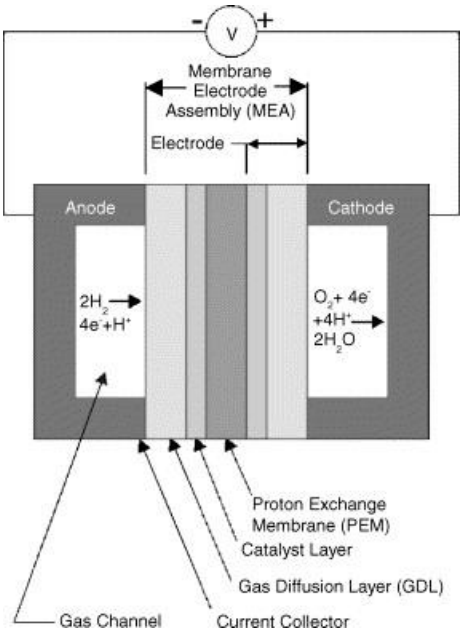

Figure 5. Schematics[23] for basic hydrogen fed PEM. Protons are able to pass the proton exchange membrane but the electrons travel via external circuit from the anode to the cathode.

The electrochemical reactions take place simultaneously on both electrodes. However, the reaction can be understood as it starts at anode catalyst interface between catalyst and membrane. The provided hydrogen through GDL is decomposed into protons and electrons (Equation 2.5.1.1). Protons then travel through the PEM to the cathode but the PEM blocks the direct movement of electrons. This prevents short circuit. Electrons move via external circuit through path of least resistance to the cathode producing electrical current. At the cathode catalyst, they come together with protons and oxygen producing final product water (Equation 2.5.1.2). [4]

$$H_2 \longrightarrow 2\,H^+ + 2\,e^- \quad (2.5.1.1)$$

$$2\,H^+ + 2\,e^- + \frac{1}{2}\,O_2 \longrightarrow H_2O \quad (2.5.1.2)$$

The overall net reaction (Equation 2.5.1.3) for typical PEM fuel cell is presented below.

$$2\,H_2 + O_2 \longrightarrow 2\,H_2O \quad (2.5.1.3)$$

Typically PEMFCs operate at temperatures between 30 and 100 °C[14].

2.5.2 Alkaline fuel cell (AFC)

One of the pioneer AFCs was developed to provide electric power for the Apollo space vehicle in the beginning of 1960. It is an archetype for a modern fuel cell. Analogously to the name the electrolyte matrix is alkaline and the charger carrier is hydroxide anion [24]. The structure is illustrated in Figure 6[25].

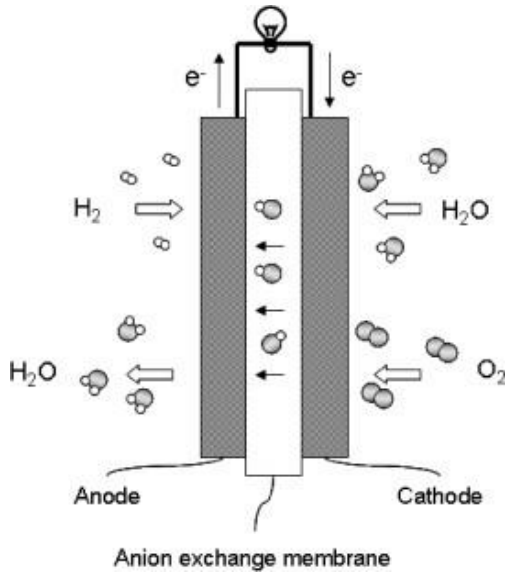

Figure 6. Schematic illustration[25] of an AFC with an anion exchange membrane (AEM).

Although, the reactions are simultaneous at cathode (Equation 2.5.2.2) and anode (Equation 2.5.2.1) similarly to PEMFCs an AFC can be comprehended working reversed in electrolyte matrix. First, at the cathode side oxygen reacts with two electrons and a water molecule producing two hydroxide ions. Next, hydroxide ions move

through the anion exchange intermediate matrix to the anode where the two hydroxide ions react with hydrogen producing water and two electrons. The two electrons move via the circuit back to the cathode generating electrical current.

$$H_2 + 2\,OH^- \longrightarrow 2\,H_2O + 2\,e^- \quad (2.5.2.1)$$

$$\frac{1}{2}\,O_2 + H_2O + 2\,e^- \longrightarrow 2\,OH^- \quad (2.5.2.2)$$

$$2\,H_2 + O_2 \longrightarrow 2\,H_2O \quad (2.5.2.3)$$

The overall reaction (Equation 2.5.2.3) is that two hydrogen gas molecules react with oxygen generating two water molecules.

AFCs typically operate in medium temperature range of 50–200 °C[14].

2.5.3 Solid oxide fuel cell (SOFC)

SOFCs, as the name suggests, uses as an electrolyte solid ceramic oxide and the charge carrier is oxide ion (O^{2-}). The ceramic layer is made of metallic oxides, like yttria-stabilised zirconia. It is crystal structure of zirconium dioxide (ZrO_2) and stabilized by adding around 8 mol-% yttrium oxide (Y_2O_3) [26]. SOFCs can make use of variety of fuels to generate electricity from common pure hydrogen to carbon monoxide, methane and other hydrocarbons[18]. The schematics for methane fed SOFC is presented in Figure 7.

The main interest in SOFC technology is that they can implement less expensive materials for electrodes such as nickel-YSZ-composite material on anodes compared to the cost of noble metals in the platinum group that are commonly used in proton carrier based PEMFC technologies. Due to high temperature and high oxidation doped materials are often preferred such as strontium-doped lanthanum manganite (LSM) in cathodes. [24]

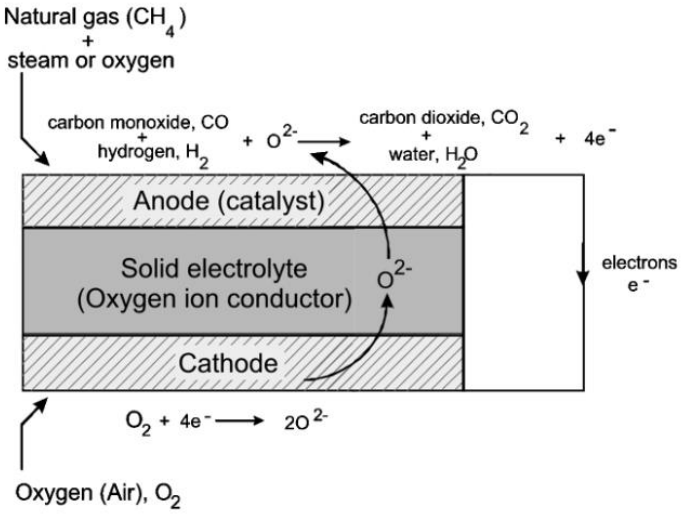

Figure 7. Schematics[26] for solid oxide fuel cell. The oxide ions are transferred from the cathode to the anode though a ceramic electrolyte.

Disadvantageously, SOFC systems require more time to cool down and heat up when compared to the other fuel cell technologies. This is particularly true in applications that require quick start-up and cool down. SOFCs operate typically at high temperatures ranging from 500 to 1000 °C[27]. [26]

2.5.4 Biological fuel cell (BFC)

Biological fuel cells are an emerging versatile and low-temperature fuel cell technology. BFCs are generally divided into two subgroups. One utilise either immobilized catalysts that are directly extracted from biological cells, potential catalysts include enzymes and even mitochondrion. The other subtype of BFC utilises metabolic processes of living microbes in order to generate electricity.

The current main interest in BFC technology is due to the possibility to generate additional cheap energy at wastewater treatment plants. Additionally, BFCs could be used to power compact biodegradable electrical devices.

However, prominent issues need to be solved before the biological fuel cell technology is ready to be accepted by the public markets. These issues are related to general operational stability, includes problems in cell voltage, current density and power density. [28]

Enzymatic fuel cell contains enzymes that provide electricity to the circuit. In most simplistic version of an enzymatic fuel cell no electrolyte membrane is needed. This is because the structure is based on two enzymes at electrodes. The first enzyme oxidises fuel (substrate) at the anode end and passes the electron to the electrode. At the cathode side the second enzyme reduces an oxidant (substrate) with the passed electron.

Electron transfer can be implemented by either direct or mediated method (see Figure 8 [28]).

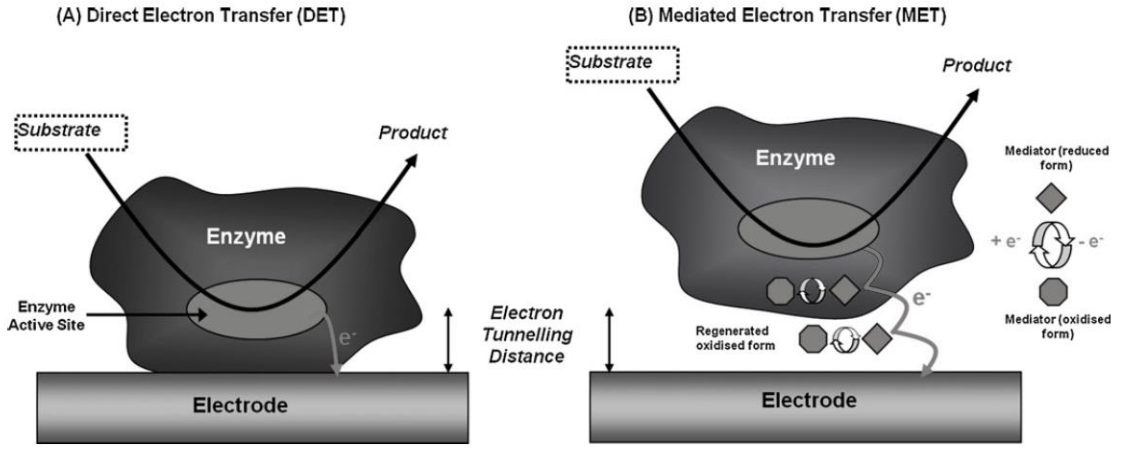

Figure 8. Illustration[28] of two different methods using enzyme for an electron transfer to the electrode. The direct electron transfer (DET) transfers directly the electron from the substrate (e.g. fuel) to the anode (A). In the other method, mediated electron transfer (MET), the mediator first grabs the electron from the substrate with greater reduction potential and then the mediator hands over the electron to the anode (B).

Redox enzymes are composed of the protein component (apoenzyme) and electroactive cofactors. The companionship of the cofactors enables successful electron transfer between the enzyme and substrate [28]. Related to the redox reactions the common cofactors in main glucose-oxidizing enzyme groups like glucose oxidases (GOx) and glucose dehydrogenase (GDH) are FAD (flavin adenine dinucleotide), NAD(P) (nicotinamide adenine dinucleotide [phosphate]) and PQQ (pyrroloquinoline quinone). It should also be added that unlike the enzymes in GOx-group the GDHs are unable to utilize oxygen in electron transfer reactions even if utilizing the same redox cofactors as GOx, which may be relevant for methods utilising MET. [29]

The other subtype of biological fuel cell is a microbial fuel cell that utilise microbes to generate electricity. Many different types of microbes can be used to power a fuel cell.

Commonly microbes either generate hydrogen to the normal hydrogen fed fuel cell or more interestingly provide directly free electrons to the fuel cell by oxidizing organic matter. However, in general biological methods for generating hydrogen should be distinguished from direct biological fuel cells and think them as some sort of reformers that provide hydrogen to fuel cells. [14]

In 2006 it was demonstrated by A. L. Walker and C. W. Walker Jr [30] that *Saccharomyces cerevisiae* is capable to run a microbial fuel cell.

The choice to use dry components including dry Baker's yeast that can be stored in dry conditions make it very fascinating idea for a compact and biodegradable fuel cell system that is ready to use after hydration.

The demonstration[30] (see Figure 9) explained that the best results in demonstration were obtained when the anode side contained 0.1 M glucose and 0.005 M methylene blue in solution. The cathode side contained equal volume 0.1 M potassium ferricyanide. Methylene blue will participate in the electron transfer reaction in ATP formation reaction by capturing an electron in reduction-oxidation reaction [31]. In the next step the methylene blue is oxidized again by losing the electron to the oxidizing agent ferricyanide via circuit. The protons are able to penetrate through the PEM electrolyte.

Although yeasts are facultative aerobes, it is theoretically desirable for a yeast based fuel cell to be running in aerobic condition for sufficient power density due to the metabolic pathways of *S. cerevisiae* (Equation 2.5.4.1, 2.5.4.2). The end products of the two reactions are different, thus directly affecting to the production of ATP (adenosine triphosphate)[32] and therefore to the number of available electrons to the electrode.

$$C_6H_{12}O_6 + 6\,O_2 \xrightarrow{\text{Yeast (aerobic)}} 6\,CO_2 + 6\,H_2O + 36\,\text{ATP} \qquad (2.5.4.1)$$

$$C_6H_{12}O_6 \xrightarrow{\text{Yeast (anaerobic)}} 2\,C_2H_5OH + 2\,CO_2 + 2\,\text{ATP} \qquad (2.5.4.2)$$

The ATP-electron ratio used in the demonstration is based on full oxidation of glucose with water (Equation 2.5.4.3). The overly simplified ATP-electron ratio is 3/2, therefore the anaerobic pathway can provide only 4/3 electrons while anaerobic pathway theoretically yields sufficient 24 electrons per glucose molecule [30].

$$C_6H_{12}O_6 + 6\,H_2O \longrightarrow 6\,CO_2 + 24\,H^+ + 24\,e^- \qquad (2.5.4.3)$$

It is advisable to note that this demands, especially in aerobic conditions, that the mediator (methylene blue) is able to capture an electron. Otherwise the electron is lost to the oxygen that is reduced and no electron is available to the ferricyanide anion at the cathode side. For this reason, the study concluded that it is the anaerobic conditions that are preferred in the fuel cell. However it was also mentioned in the study that the preferred conditions may change if the fuel cell is operating longer periods of time. [30]

Additionally, it should be emphasized that the choice of mediators is limited because the hydrophilic mediators cannot penetrate the cell membrane of a eukaryotic (e.g. yeast) cell. Lipophilic mediators are able to access the catabolic redox sites in cytoplasm and mitochondria in eukaryote cells. Although hydrophilic mediators are able to access the major catabolic redox sites in a prokaryotic cell (e.g. bacterium). [33]

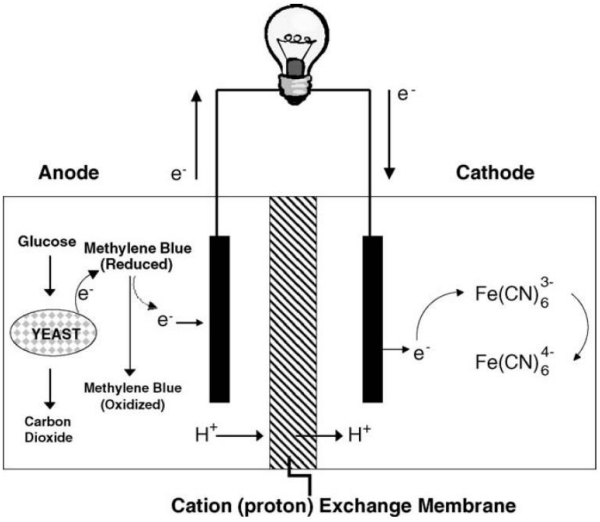

Figure 9. Schematics for the microbial fuel cell by A. L. Walker and C. W. Walker[30].

Microbial fuel cell technologies based on reducing bacteria without mediators are also presented[34]. The microbial fuel cells are still generally at concept level but they do offer an interesting take on generating electricity especially disposability in mind. However, the general issues are the same as presented in the beginning of this chapter related to operational stability.

2.6 Proton exchange membrane direct methanol fuel cell (PEMDMFC)

Methanol is fairly rich source of hydrogen and sometimes used in fuel cells instead of hydrogen for practical and safety reasons. Advantages for using methanol include that methanol is in liquid form at standard pressure and temperature range of -97 °C and 65 °C making it denser than hydrogen gas. However safety-wise it cannot be unanimously said that methanol is safer option, for example in enclosed space hydrogen is considered to be even safer option by some. [35]

PEM technology is currently the most typical in methanol fuel cells[6]. Additionally, AFC-based DMFCs are proposed [24]. DMFCs in general typically operate at lower temperatures, 20–90 °C[14].

Similarly, to the PEMFCs, the PEMDMFCs utilise proton exchange membrane as an electrolyte but is fed with methanol instead of hydrogen. Despite the compact size of DMFC, the use of rare noble metals such as platinum and ruthenium in the catalyst layer make the DMFCs fairly expensive [6] for disposable products.

Platinum used on the anode catalyst (Equation 2.6.1) layer catalyses the oxidation of aqueous methanol fuel mixture into desired electrons and protons, and additionally into carbon dioxide [36]. The protons move through the electrolyte membrane and electrons move via circuit generating electricity. At the cathode (Equation 2.6.2) catalyst layer the atmospheric oxygen reacts with electrons and protons producing water [37]. This leaves the overall cell net reaction (Equation 2.6.3) for the DMFC. More precise reaction pathways with platinum and ruthenium catalysts are presented in chapter 2.8.2.

$$CH_3OH + H_2O \longrightarrow CO_2 + 6\,H^+ + 6\,e^- \tag{2.6.1}$$

$$6\,H^+ + 6\,e^- + \frac{3}{2}\,O_2 \longrightarrow 3\,H_2O \tag{2.6.2}$$

$$2\,CH_3OH + 3\,O_2 \longrightarrow 2\,CO_2 + 4\,H_2O \tag{2.6.3}$$

The component structure (see Figure 4 in chapter 2.5) in PEMDMFC is homologous to PEMFC. This structure is represented with function compartments in Table 3.

Table 3. Different compartments in methanol fuel cell with their primary functions listed

Compartment	Description	Typical material (material property needs)
Anode current collector	Conducts current	N/A (high conduction, inert for reactions)
Anode flow channel	Sealing layer	Carbon/plastic (input for methanol aq., output for carbon dioxide)
Anode gas/liquid diffusion layer	Diffusion layer	Carbon fabric (diffusion, electric conductivity, heat transfer, mechanical strength)
Anode catalyst layer	Catalyst layer	Platinum (redox reaction catalysis, methanol oxidation)
Membrane layer	Active membrane for charge carrier	Nafion (prevent the flow of charged particles except carrier particles, e.g. protons)
Cathode catalyst layer	Catalyst layer	Platinum (redox reaction catalysis, oxygen reduction)
Cathode gas diffusion layer	Diffusion layer	Carbon fabric (diffusion, electric conductivity, heat transfer, mechanical strength)
Cathode flow channel	Sealing layer	Carbon/plastic (input for oxygen, output for water)
Cathode current collector	Conducts current	N/A (high conduction, inert for reactions)

Methanol fuel cells can either be direct or indirect. DMFC means that the methanol is oxidised directly. Alternatively, indirect methanol fuel cells (IMFC) utilise some sort of a reformer. Methanol reformer is a device that converts methanol and water into hydrogen and carbon dioxide. Alternative name for reformer based methanol fuel cells is reformed methanol fuel cell.

2.7 Carbon monoxide poisoning (CMP)

Carbon monoxide (CO) is a small bipolar molecule and it behaves in some cases similarly to bipolar water molecule. Those characteristics make carbon monoxide able to penetrate PEM, which leads to loss in fuel and mixed potential at the air cathode.

Increased total pressure and lower relative humidity increases the carbon monoxide equilibrium concentration through chemical reaction presented in Equation 2.7.1. Although not much data is available of CMP in low temperature PEMDMFC, it is reported that PEM-based hydrogen fed fuel cells tend to tolerate higher concentrations of carbon monoxide at higher temperatures. This is can be explained by the increased partial pressure of water that reduces the concentration of carbon monoxide[38] in equilibrium. [27]

$$CO_2 + H_2 \longrightarrow CO + H_2O \quad (2.7.1)$$

$$CO_2 + 2\,H^+ + 2\,e^- \longrightarrow CO + H_2O \quad (2.7.2)$$

In literature is reported that CMP can occur on platinum at both electrodes reducing the overall cell performance. This is reported to occur with carbon monoxide levels as low as 1 ppm[39] in hydrogen fuel cells. It is also reported that with concentrations of 10 ppm carbon monoxide it took approximately 120 minutes to carbon monoxide cover half the platinum adhesion sites and 360 minutes to take full coverage [40]. More resistant platinum alloys such as platinum-ruthenium and platinum-molybdenum can tolerate carbon monoxide concentrations of 20-50 ppm and the electrical potential drop is not as steep compared to pure platinum.

In relation to CMP carbon dioxide may be reduced to carbon monoxide (Equation 2.7.2) at voltages over 0.6 V, this phenomenon is directly referred as carbon dioxide poisoning[41], although, essentially it is carbon monoxide poisoning. In passive fuel cells the oxygen is most likely taken from air. Composition of air[42] (see Table 4) contains approx. 330 ppm carbon dioxide, which is most probably trivial due to the low ratio of reduced carbon dioxide[39]. Moreover, Equation 2.7.1 is believed to be more prevalent than Equation 2.7.2 because it requires only contact with catalyst site and gases whereas the latter reaction demands gas, ionic and electronic access.

Table 4. Composition of dry air[42]. Additionally, air contains water vapour depending the temperature and humidity, it is commonly varying between 0.1 % and 6 % of total volume.

Substance	Volume-%
Nitrogen (N_2)	78.08
Oxygen (O_2)	20.95
Argon (Ar)	0.93
Carbon dioxide (CO_2)	0.033
Neon (Ne)	0.0018
Helium (He)	0.00052
Methane (CH_4)	0.0002
Krypton (Kr)	0.00011
Nitrous oxide (N_2O)	0.00005
Hydrogen (H_2)	0.00005
Xenon (Xe)	0.0000087
Ozone (O_3)	0.000001

Related to carbon monoxide poisoning, it is suggested that methanol oxidation typically results a gas mixture approximately 74 % hydrogen, 25 % carbon dioxide and 1–2 % carbon monoxide [41].

2.8 Membrane electrode assembly (MEA)

Membrane electrode assembly (MEA) is a term for describing assembled fuel cell stack structure with an electrolyte membrane. The end number refers to the number of layers. In MEA-3 form (see Figure 10, MEA-3) it contains a membrane (B) with two catalyst layers on both opposite planes (A) forming an anode and a cathode to the fuel cell. Alternative name for the explained MEA-3 structure is catalyst coated membrane (CCM). [43]

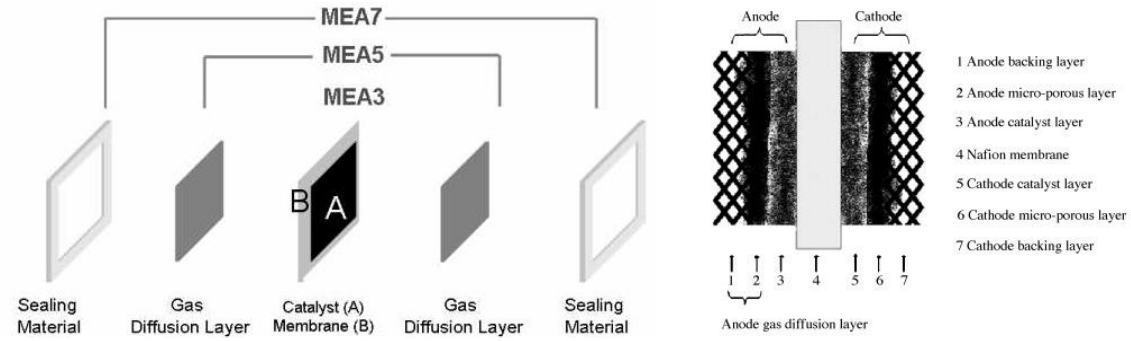

Figure 10. Illustration[44] of membrane electrode assembly and layers in Nafion based DMFC[45].

In MEA-5 (see Figure 10 MEA-5) porous GDL is added to MEA-3. GDL provides high thermal and electrical conductivity and allows proper flow for the fuel and atmospheric oxygen to catalysts. It also removes efficiently the fuel oxidation by-products, e.g. water and carbon dioxide from the fuel cell. It is commonly untreated carbon paper or carbon cloth but can be wet-proofed for example with PTFE. [44,45]

MEA-7 adds sealing layers to MEA-5 assembly. Sometimes it is referred as edge-sealed MEA-5 [43]. Sealing layer is often added to resist deformation, i.e. to support the rigidity of assembly. Layer structure is presented at right in Figure 10.

2.8.1 Electrolyte membrane materials

Electrolyte is the intermediary layer in a MEA. The most important properties for the electrolyte membrane are the ability to provide infrastructure for the carrier particles to travel between the two electrodes and also prevent the direct flow of electrons through the membrane from anode to cathode, which would result to short circuit. Additionally, membrane should prevent methanol crossover from anode to cathode, which results mixed potential reducing electric potential of the fuel cell and cause loss of fuel.

In PEM-based DMFC designs the most typical material for the electrolyte layer is poly-perfluorosulfonic acid such as Nafion. Nafion is currently considered the state-of-the-art material for proton exchange membrane[46].

Nafion (see Figure 11) is perfluorinated ion-exchange membrane and a registered trademark of The Chemours Company FC, LLC. Chemours is DuPont's spin-off company.

Nafion provides a solid and stable superacidic (compared >100 % H_2SO_4) environment for successful proton conductivity that can, in some extend, to be attributed to the backbone perfluorocarbon chain interacting with the sulfonic group. Perfluorocarbon chain favours the mobility of protons, therefore increasing the tendency to sulfonic acid to lose a proton[47]. However Nafion is neither hazardous nor corrosive chemical [48]. Nafion is stable for oxidation, which is important in fuel cell environment[46].

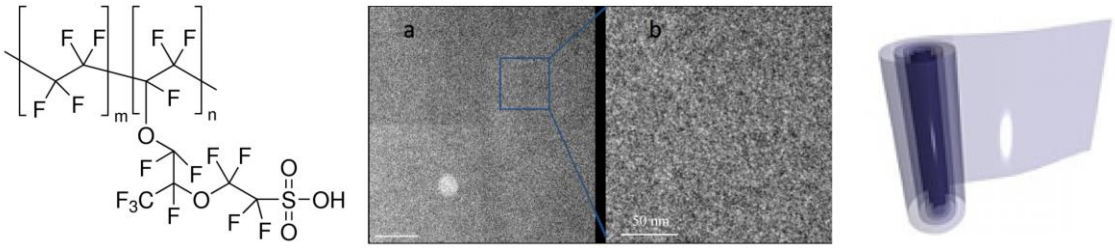

Figure 11. Chemical structure of Nafion polymer containing sulfonic acid as a functional group (left) [49]. Latin alphabets m and n imply the molar compositions of copolymers, not the length of sequence. Bright field TEM images of undamaged membrane (middle, a) and 4x section magnification (middle, b) [50]. Picture[51] of a Nafion sheet roll (right).

Currently Nafion is most commonly supplied at equivalent weight of 1100 g (87 mol-%) per sulfonic acid group and in approximated thicknesses of 50 µm (N112), 125 µm

(N115), 175 µm (N117) and 255 µm (N1110). However different compositions of copolymers are commercially available as the ion exchange specifications can be modified by altering the ratio of copolymers [46].

The problem using perfluorinated hydrocarbons in DMFCs is that the methanol diffusion is high. Methanol crossover is reported to be as high as 40 % [52]. It is also noted that Nafion dehydrates at environments with temperatures over 80 °C and relative humidity below 100 %. Dehydration reduces the ionic conductivity for protons in Nafion membrane. Solution-cast Nafion membranes with carefully selected dispersants are presented to overcome these problems, although more research is still needed. Additionally the synthesis of Nafion is laborious and the current costs for raw materials are undesirable making Nafion expensive [46]. [53,54]

Nafion is typically prepared before using it as electrolyte membrane. The preparation can be done by boiling Nafion in 3 wt. % hydrogen peroxide (H_2O_2) solution for 1 hour and then in deionised water (DIW) for another 1 h. Next membrane's proton exchange properties are activated by boiling in 0.5 M sulfuric acid (H_2SO_4) solution. Finally, the residual sulfuric acid is removed by washing Nafion by boiling it again in DIW. [55]

In literature is suggested that cells operating with lower methanol concentrations (2.0 M) and lower current densities benefits from thicker membrane. However, at higher current densities the thinner layer turned out to produce better performance. At higher methanol concentrations (4.0 M) cells yielded similar voltages. Overall thicker membranes exhibited higher efficiencies. [56]

2.8.2 Electrode catalyst layer materials

Material selection is important in catalyst layer. The properties of the selected materials need to offer good capacities for electric transfer. It is also important that the material allows good methanol and oxygen intake and outtake for waste products such water and carbon dioxide to support optimal reaction environment. Similarly, adequate gas exhaust to other molecules not used in reaction, e.g. atmospheric nitrogen, is important.

Electrocatalyst layers provide an environment that support sufficient kinetics of redox reaction. Most common catalysts are platinum and ruthenium. Such catalyst layers can

be produced by using either impregnation or colloidal dispersion for carbon black. The problem with impregnation is that high dispersions are hard to achieve with high metal catalyst concentrations. Alternatively, colloidal method offers higher surface area with high metal catalyst loading but generally it has higher complexity of the formulation and preparation. [57]

Platinum is highly dense, soft and silvery white noble metal, and part of six metals in platinum group metals. Platinum is considered more precious than gold because it is more expensive to produce pure platinum than gold. It is used in wide variety of applications from the decorative items to industrial items, it is estimated that around one fifth[58] of all the goods made in factories in the US the platinum is involved either directly in the product material or used as part of the processing as catalyst. [59]

Chemically platinum is very unreactive metal. Platinum dissolves into temperated aqua regia to form chloroplatinic acid. It resists well corrosion by water, oxygen or other chemicals even at high heat. Still, some halogens, cyanides, sulphur and strong corrosive alkalis can corrode platinum. [59,60]

Platinum is important in low temperature fuel cells, because it is needed to catalyse the redox reaction between oxygen and methanol. It allows the momentary adhesion of hydrogen atom. Fuel cell technologies that operate at higher temperature (>600 °C) such MCFC and SOFC can achieve adequate reaction rate without platinum catalyst[14].

Basic mechanism for platinum in methanol electro-oxidation reaction is presented below via widely believed adsorption intermediates forming exhaust carbon dioxide. First, methanol is adsorbed to platinum surface. Then hydrogens of methanol is oxidised (Equation 2.8.2.2–2.8.2.4). [61]

$$CH_3OH + Pt(s) \longrightarrow Pt\ CH_2OH + H^+ + e^- \quad (2.8.2.1)$$

$$Pt\ CH_2\mathrm{OH} + \mathrm{Pt(s)} \longrightarrow Pt_2\ \mathrm{CHOH} + \mathrm{H^+} + \mathrm{e^-} \quad (2.8.2.2)$$

$$Pt_2\ \mathrm{CHOH} + Pt(s) \longrightarrow Pt_3\ \mathrm{COH} + \mathrm{H^+} + \mathrm{e^-} \quad (2.8.2.3)$$

$$Pt_3\ \mathrm{COH} \longrightarrow Pt\ CO + 2\ Pt(s) + \mathrm{H^+} + \mathrm{e^-} \quad (2.8.2.4)$$

The both pathways for post-intermediates are possible (Equation 2.8.2.6-A and 2.8.2.6-B), although it is suggested that methanol oxidation favour the latter with water co-adsorbed. Additionally, other post-intermediates are suggested trough HCHO and HCOOH. Finally, carbon dioxide is desorbed (Equation 2.8.2.7). Post-intermediate reactions need an oxygen donor, e.g. water (Equation 2.8.2.5).

$$Pt(s) + H_2O \longrightarrow Pt\,OH + H^+ + e^- \quad (2.8.2.5)$$

$$Pt\,OH + Pt\,CO \longrightarrow Pt\,COOH \quad (2.8.2.6\text{-A})$$

$$Pt\,CO + H_2O \longrightarrow Pt\,COOH + H^+ + e^- \quad (2.8.2.6\text{-B})$$

$$Pt\,COOH \longrightarrow Pt(s) + CO_2H^+ + e^- \quad (2.8.2.7)$$

Finally, univalent aldehyde is desorbed freeing the active binding site on platinum catalyst (Equation 2.8.2.7).

Furthermore, it should be noted that pre-intermediates require free platinum neighbours at surface and voltages near 0.2 V/RHE to occur. Post-intermediate reactions need the presence of water and voltages above 0.4–0.45 V/RHE. However, pure platinum does not provide good reactivity below voltages 0.7 V/RHE. [62]

Pure platinum is vulnerable to carbon monoxide poisoning that occurs commonly at anode in methanol fuel cells. CMP is caused either by incomplete oxidation of methanol or the reduction of carbon dioxide at voltage range 0.6–0.9 V and above. It reduces fuel cell's electric potential and energy conversion efficiency [41]. Carbon monoxide poisoning is discussed in chapter 2.7.

Alternative materials for fuel cell catalysts are investigated due to rarity and expensive nature of platinum.

Ruthenium is fairly expensive and silvery white metal in platinum group. It is effective for reducing nitrogen monoxide (NO) in reactions with carbon monoxide and hydrogen gas. Although in fuel cells more commonly ruthenium is added to reduce carbon monoxide poisoning of platinum. Carbon monoxide poisoning is because the carbon mon-

oxide is adsorbed to the surface of platinum, therefore reducing the number of active catalyst sites on platinum for redox reaction, see chapter 2.7.

The protective chemical mechanism of ruthenium can be presented in two equations. First, the ruthenium activates water molecules on the surface forming hydroxide. Next the formed hydroxide oxidizes the carbon monoxide on the platinum producing carbon dioxide. [62,63]

$$Ru(s) + H_2O \longrightarrow Ru\,OH + H^+ + e^- \quad (2.8.2.1)$$

$$Pt\,CO + \mathrm{Ru\,OH} \longrightarrow CO_2 + H^+ + e^- + \mathrm{Pt(s)} + Ru(s) \quad (2.8.2.2)$$

Added ruthenium increases the rate of freeing active but occupied catalyst sites on platinum.

2.8.3 Gas diffusion layer (GDL) materials

Main importance of GDL is to provide a stable medium to that provides good gas diffusion for fuel cell by transporting reactant gasses and removing water. GDL should also provide low resistance for electron conductivity. [64]

Carbon is often used due to the fact that it is inexpensive, extremely versatile and abundant material on Earth. Although, synthetic carbon products especially carbon nanotubes are still fairly expensive even at bulk quantities.

Carbon black refers to industrial products that essentially consist of near spherical colloidal sized particles of carbon. They are produced by partial or thermally controlled combustion of various hydrocarbons, often preferably aromatic hydrocarbons. Traditionally it is used as black pigment in ink. [65].

Literally, graphene is a term for infinite hypothetical two-dimensional layer of sp^2-crystalline carbon in hexagonal lattice. Although, commonly a layer of graphite is referred as graphene sheet. The naturally occurring three-dimensional counterpart is graphite. It is the most stable form of carbon in STP conditions. Graphite offers high thermal stability and electrical conductivity but oxidizes at around 800 °C with oxygen in air. [66]

Carbon nanotubes (CNT) are cylindrical nanostructures for carbon allotropes of fullerene family. The properties include exceptional tailorable heat and electric conductivity and the hollow structure of a cylinder can offer benefits for the controlled fluid flow through the material[67]. Generally, carbon nanotubes are formed by rolling graphene at specific angles (see Figure 12, A), which contributes directly to their diameter, but the total spectrum is extremely broad. Multi-walled nanotubes are complexes of multiple nanotubes put together by making the innermost tube smallest and outermost largest by diameter. [68]

The diameter of carbon nanotubes varies by the structural composition, typical outer range is between 0.8 nm to 20 nm, but is not limited and currently multi-walled nanotubes can exceed 100 nm. One study found that single-walled nanotubes that had an outer diameter of 1.85 nm had the inner diameter around 1.7 nm[69]. This potentially allows pathways for exchange gases associated to methanol fuel cells such nitrogen, carbon dioxide and oxygen based on their kinetic diameters [70] that are in ranges below 1 nm. Naturally, potential buckling[68] under strain reduces the diameter in carbon nanotube. The CNT lengths can vary between 100 nm to centimetres and beyond. [71]

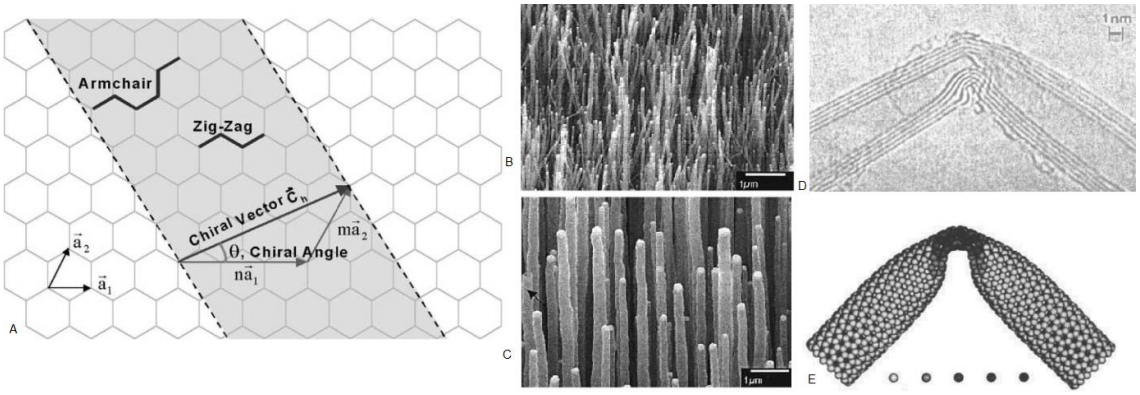

Figure 12. Schematic (A) showing the orientating aspects for rolling a single layer graphite into a CNT. Micrographs (B and C) demonstrate the stability of the outer diameter in CNTs, the long axis vertically oriented. Scale is 1 µm. TEM micrograph (D, scale 1 nm) and simulation rendering (E) showing the buckling. [68]

Carbon fibre is usually a fibre that is made by stacking graphite sheets parallel to another. Weak intermolecular forces keep the sheets in place and form a solid structure. Alternatively, carbon fibre can be carbon nanotube or any other relatively long structure of pure carbon.

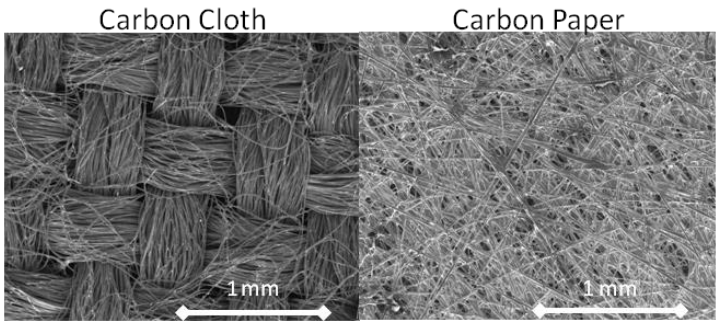

Figure 13.Two micrographs to illustrate the difference between woven (left) and non-woven fabric (right). [72]

Carbon fabric such as cloth or paper is a combination of anisotropic carbon fibres that provide conductivity and structural porosity for sufficient diffusion of gases. It is often used as material of choice to GDL [73]. Non-woven fabric is often considered carbon paper and cloth is woven. Typically carbon cloths are thicker and offer more flexibility[72]. Carbon cloths are generally also more robust compared to more brittle carbon papers. In the end all properties come to the type of used fibres in fabric and the fabric structure contributes to the properties of carbon fabric.

2.9 Fuel cell construction techniques

2.9.1 Inkjet printing (IJP)

Inkjet printing is a technique used for depositing liquid phase material on substrate. The printing material, ink, consists of solvent component and dispersed solute. In the last few decades IJP has matured to the point where it is has become interesting and capable tool for printing different functional materials on many kinds of substrates. IJP is widely studied technology and the possibilities to print electrically conductive microstructures directly to substrates make it rapid and adequate technique for quick prototyping.

The advantages of IJP include minimal material consumption and flexibility to print various materials, e.g. organic diodes or transistors[74]. It is possible to print multiple layers on top of other layer. [75]

The general idea behind IJP is that a fixed amount of ink is ejected from a print-head nozzle. The two main inkjet printing technologies are continuous inkjet (CIJ) and drop-

on-demand inkjet (DOD). CIJ is mainly used for printing coding and information markings on packages, whereas DOD is more familiar with office and home printing as well as for industrial printing, including large format graphics printing. DOD printing technology can further be divided into thermal inkjet and piezoelectric inkjet printing, and the latter is used for printing functional materials.

The mechanism behind the ejection in piezoelectric print heads is based on pressure waves, i.e. shockwaves. The shockwaves are generated by using piezoelectric material that changes its dimensions when electrical field is applied. After an ink droplet is pushed out of the nozzle, the droplet fall is affected by air resistance and gravity until the droplet hits the substrate and spreads. The formation of a viscous ink droplet is presented in Figure 14. Finally the droplet adheres to the substrate due to wetting penetration and drying trough solvent evaporation forming the final print shape. [76]

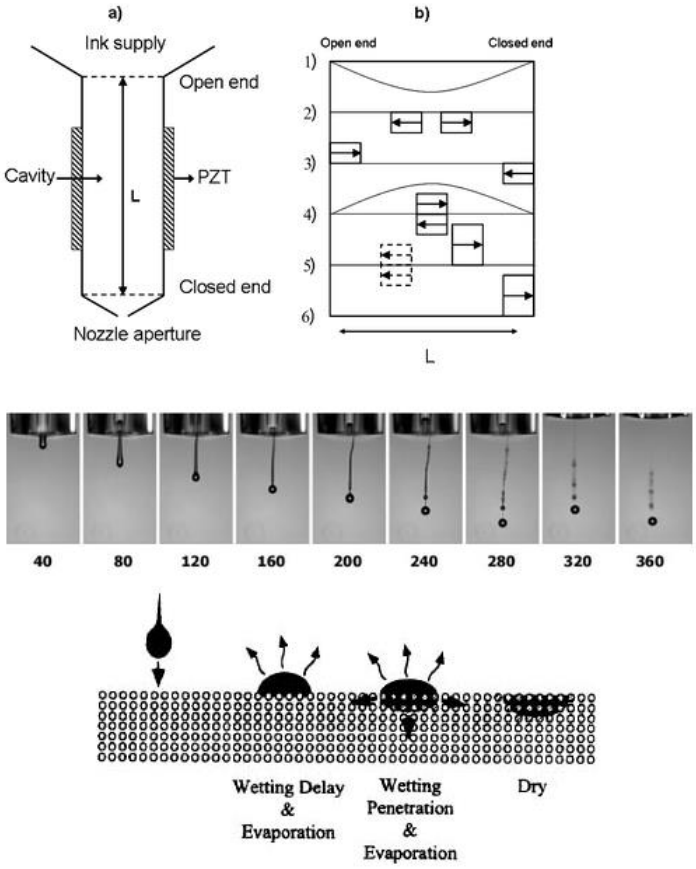

Figure 14. Illustration (top left) of piezoelectric inkjet print head and presentation of shockwave mechanism (top right) inside the nozzle cavity. Droplet formation (middle) of an ink (polystyrene in acetophenone) droplet[77] as a function of time (µs). General ink drying process (bottom) [78]. [79]

In general droplet ejection cycle starts when electrical voltage is applied. Applied voltage causes the piezoelectric material (e.g. PZT) to expand increasing the diameter of the nozzle cavity (Figure 14 b, 1). This generates a negative shockwave to the liquid that splits into two smaller waves with half amplitude and opposite directions. The shockwaves then travel to the open and closed terminals (Figure 14 b, 2). The wave travelling to the closed terminal is reflected back from the closed end, while the other shockwave hitting to the open end is reflected back in reversed phase (Figure 14 b, 3). [80]

Voltage is next dropped when the two shockwaves meet in the centre of nozzle cavity (along L axis in Figure 14 b, 4) causing the cavity diameter decrease now. This sudden decrease in volume generates a positive shockwave that interacts with the two former shockwaves. The former negative shockwave is destructed and the former positive shockwave is constructed (Figure 14 b, 5) to the new generated positive shockwave. The newly generated positive shockwave with doubled amplitude is travelling to the nozzle tip pushing the fluid outwards (Figure 14 b, 5). [79]

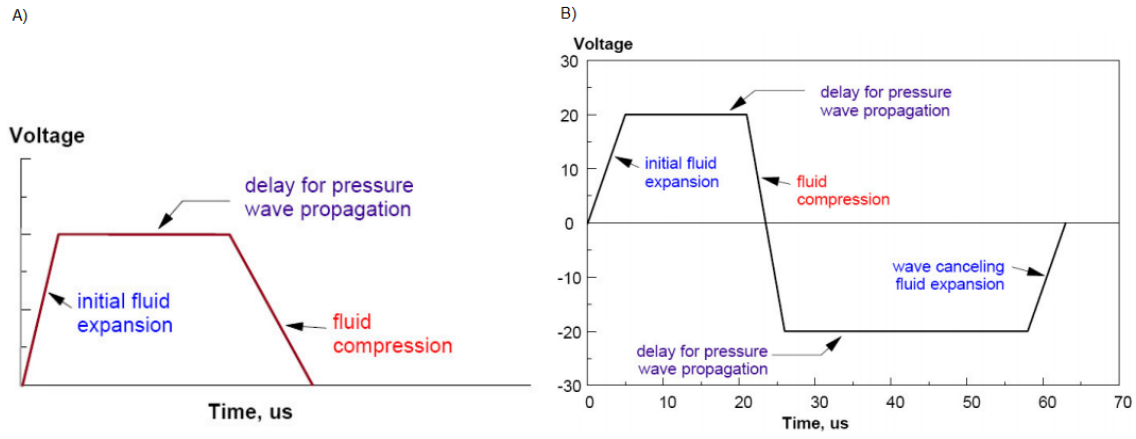

Figure 15. Graph (A, left) is presented the simplest on-off pulse. Graph (B, right) shows a sample of more complex waveform that takes residual vibration in consideration. Vertical axis presents voltage and horizontal axis time in microseconds. [81]

The most basic jetting waveform resembles trapezoidal function; however, many different ink properties should be taken in consideration (see Figure 15) when generating jetting waveform. For example, viscosity, residual vibration and surface tension of ink affect to the stability of droplet formation and therefore complicating the ink flow. All these properties affect the overall print quality. [81]

2.9.2 Passive PEMDMFC MEA design

Multiple stack designs are presented in literature for a functional passive PEMDMFC MEA. Optimal stack design is important for fuel cell functionality. It enables the separated components to work together. This chapter presents some of those found in literature. Summary can be found in Table 5.

In a study by Falcão et al[82], four MEAs were produced with different materials in membrane and gas diffusion layer. However, catalysts loadings in anode and cathode were identical in all MEAs, respectively, 3 mg/cm^2 Pt/Ru and 0.5 mg/cm^2 Pt-B loadings. Anode gas diffusion layers (AGDL) were constructed in all MEAs identically using unhydrophobised carbon paper (Freudenberg H2315). However, in cathode gas diffusion layers (CGDL) different two types of carbon paper (Freudenberg H2315 with hydrophobised MPL and Sigracet 10 BC 5 % hydrophobised with MPL) were tested. Both CGDL choices were tested with Nafion 117 and Nafion 115 membrane. MEAs were constructed between two acrylic end plates. Anode plate contained methanol reservoir and cathode plate was opened for air diffusion. Two silicon gaskets were also used.

Y. Tang et al[55] used two different openings at current collectors for testing free open ratio (38.5 % and 28.3 %) influence to methanol and air diffusion. Additionally, these were tested by using two different construction methods. The first type used hot pressed diffusion layer (HPDL) that was pressed together at 120 °C and 10 MPa for 2 min. The second type used non-bonded diffusion layer (NBDL). See Figure 16. Both construction approaches were also tested with three different thicknesses of Nafion membrane; Nafion 212, Nafion 115 and Nafion 117. Catalysts layers were coated with 4 mg/cm^2 Pt-Ru (nominal 1:1) at anode and 2 mg/cm^2 Pt at cathode. Diffusion layers were composed of TGP-H-060 carbon paper coated with PTFE/C mixture medially towards the electrolyte. Study concluded that higher open ratio provides better mass transfer and helps gas exhaust. However, on the flipside, it also increased methanol consumption and cross-over, thus reducing efficiency. NBDL MEA exhibited similar properties increasing mass transfer versus HPDL MEA.

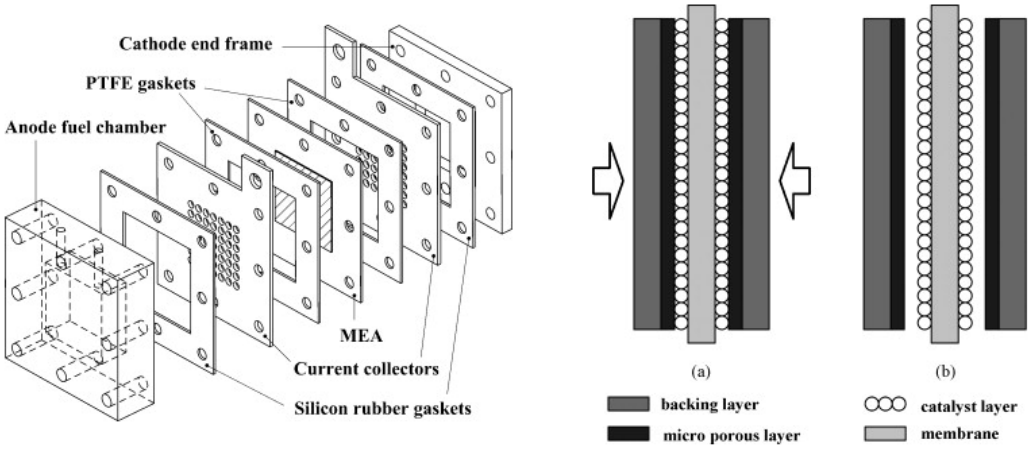

Figure 16. Schematics for PDMFC configuration used in study by Yong Tang et al (left) and hot pressed diffusion layer (right, a) and non-bonded diffusion layer (right, b). [55]

Study published by O. Barbera et al[83] presented a stack design utilising doctor blade technique to rotogravure catalyst layers directly on diffusion layers. In mini-stack design (see Figure 17) at anode they used Pt-Ru mixed with 15 wt. % Nafion ionomer solution printed on 360 µm thick GDL and at cathode Pt mixed with 15 wt. % Nafion ionomer to 280 µm thick GDL. Nafion 115 served as a membrane. Carbon cloth was used as backing material. MEAs were hot pressed at 130 °C and approx. 2 MPa for 3 minutes. Unfortunately, more exact specifications for the mini-stacks design are not published. However, for larger tested bipolar stacks in the same study they reported using catalyst loadings of 1.8 mg/cm^2 Pt-Ru/C (Pt-Ru 1:1) and 1.2 mg/cm^2 Pt/C respectively for anode and cathode. GDL material was SGL35DC. Similar to mini-stack design Nafion 115 was used as a membrane.

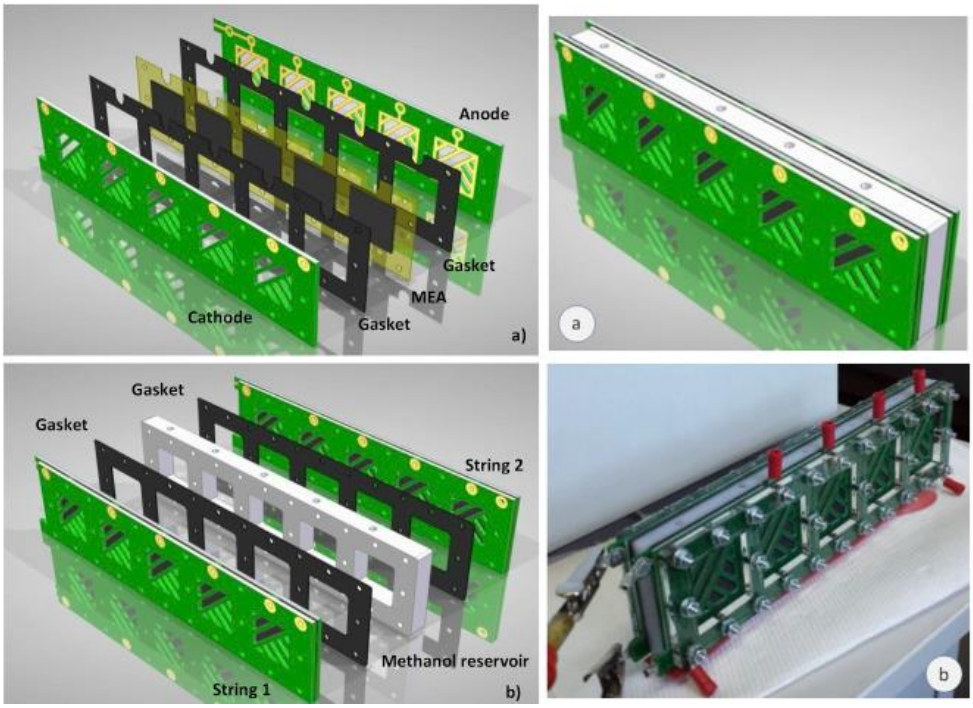

Figure 17.Design presented in a study published by O. Barbera et al. Single string assembly (top left, a) and two string assemblies with methanol reservoir in the middle (bottom left, b). Assembled mini-stack design (top right, a) and mini-stack built (bottom right, b). [83]

X. H. Yan et al[84] reported that methanol cross-over can be reduced by implementing a graphene monolayer between two thin Nafion 212 membranes to constitute more methanol resistant electrolyte layer. Commercial electrodes from Johnson Matthey were used. At anode the catalyst layer consisted of Pt-Ru/C (Pt-Ru 50%:25%) and at cathode Pt/C (60 %), loadings were respectively 4.0 mg/cm^2 and 2.0 mg/cm^2. For GDLs at both electrodes SGL carbon paper treated with 5 wt. % PTFE and a MPL were used. Anode, electrolyte membrane and cathode were sandwiched using hot pressing at 135 °C and 3.0 MPa for 3 min.

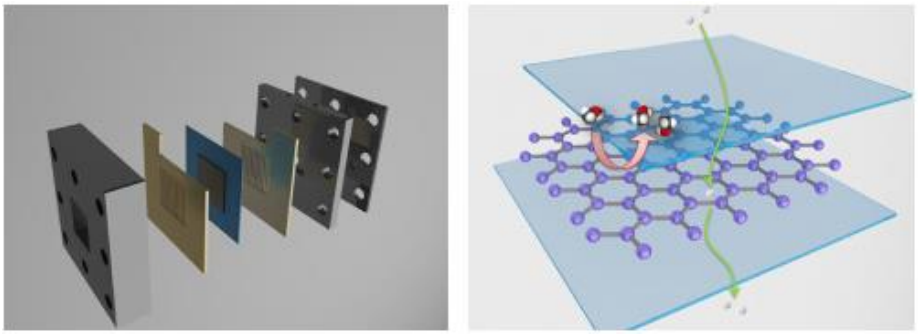

Figure 18. Setup for PDMFC (left) and schematic illustration for graphene between two Nafion membranes (right). [84]

Yang[85] et al presented a fuel cell design with separate methanol delivery system on top. MEA-3 stack was build using Nafion 117 membrane with catalyst loadings of 2 mg/cm^2 Pt-Ru/C (Pt-Ru 1:1) and 2 mg/cm^2 Pt/C to anode and cathode, respectively. Carbon paper (E-TEK B-1 Type A) was used for AGDL and carbon paper (E-TEK ELAT LT1400) for CGDL. Current collectors were made of stainless steel.

Table 5. Different MEA designs presented in literature

Reference	Membrane	Anode loading	ACL material	Cathode loading	CCL material	AGDL material	CGDL material
O. Barbera et al 2016	Nafion 115	1.8 mg/cm2	Pt-Ru/C (Pt:Ru 1:1)	1.2 mg/cm2	Pt/C	SGL35DC	SGL35DC
D.S. Falcão at al 2014	Nafion 117	3 mg/cm2	Pt-Ru	0.5 mg/cm2	Pt-B	Freudenberg H2315 (UHP)	Freudenberg H213 with MPL (HP)
Y. Tang et al 2010	Nafion NR212, Nafion 115, Nafion 117	4 mg/cm2	Pt-Ru (Pt:Ru 1:1)	2 mg/cm2	Pt	PTFE/C layer with TGP-H-060 (BL)	PTFE/C layer with TGP-H-060 (BL)
X.H. Yan et al 2016	2 x Nafion 212, graphene film sandwiched	4 mg/cm2	Pt-Ru/C (Pt 50 %, Ru 25 %)	2 mg/cm2	Pt/C (Pt 60 %)	SGL carbon paper (5 wt. % PTFE) with MPL	SGL carbon paper (5 wt. % PTFE) with MPL
Y. Yang et al 2007	Nafion 117	2 mg/cm2	Pt-Ru/C (Pt:Ru 1:1)	2 mg/cm2	Pt/C	E-TEK B-1 Type A	E-TEK-ELAT LT1400-W

*ACL anode catalyst layer, CCL cathode catalyst layer, HP hydrophobised, UHP unhydrophobised, BL backing layer

In reviewed material, the anode Pt-Ru/C loadings are between 1.8 to 4 mg/cm^2. At cathode pure platinum with carbon black and smaller amount is typically used 1.2 to 2 mg/cm^2. Additionally, MEA is commonly hot pressed tightly together. It is essential that anode and cathode catalyst layers are in direct contact with electrolyte membrane. In

literature, it is also suggested that Nafion (e.g. 0.6 mg/cm^2) should be added to catalyst layer loadings to improve proton conductivity[23]. It is also presented that low pure platinum loadings like 0.04 mg/cm^2 exhibited dramatic increase in resistance due to lower active area of catalysis compared to commercial MEA with 0.4 mg/cm^2 of pure platinum loading. However in lower-power applications (200 mA/cm^2) MEA with 0.04 mg/cm2 loadings featured decent power density of 160 mW/cm^2, although, it should be noted that these were measured using hydrogen feeding. [86]

Pt-Ru ratios of 25:1 are also suggested to show better electrocatalytic activity and carbon monoxide resistance compared to Pt-Ru ratios of 1:1, 1:0 and 1:3. The most optimal ratios are still under debate and more research is needed.

3 Experimental

3.1 Materials and methods

3.1.1 List of materials and equipment

All relevant materials used in this work are presented in Table 6 and used equipment and accessories are presented in Table 7.

Table 6. List of materials.

Supplier	Material	CAS No.	Product No.	Lot No.
Quintech	C-30/15-PT/RU	Mixture	43990	23239
Fuel Cell Store	Vulcan XC-72R	1333-86-4	590106-1	1584452-1700
Aldrich	Nafion 5 wt. % perfluorinated resin solution	31175-20-9	274704	MKBS6176V
Aldrich	4-Hydroxy-4-methyl-2-pentanone (Diacetone alcohol)	123-42-2	H41544	STBF9927V
PSG Group	Melinex ST506 (PET)	N/A	PE153-125-RL	N/A
Testbourne ltd	Gold	7440-57-5	G4-5005-M	W41015-6
Fuel Cells Etc	Nafion 117	31175-20-9	N117	1509F54345
Fuel Cell Store	Toray carbon paper 060	7782-42-5	591037	1855-2
Rathburn	Methanol	67-56-1	RH1019	13H28FA
Fluka	Sulfuric acid	7664-93-9	258105	BCBF3336V

Table 7. List of equipment and accessories.

Manufacturer	Model	Equipment	ID
IKA	T 25 Basic	Homogenizer	N/A
Branson	Digital Sonifier 450	Sonifier	TL06057
Fujifilm	DMP-2831	Materials printer	TL12681
VTT	Thermal evaporation system	Evaporator	TL14967
Ivium Technologies	Iviumstat	Potentiostat	TL02668
Bio-Logic SAS	VMP Potentiostat	Potentiostat	TL14974
IKA	VWR Lab Dancer S40	Vortex mixer	TL12979

Manufacturer	Accessory	Equipment	Product No.	Lot No.
Whatman	Rezist 30 / 1.0 PTFE	1.0 µm filter unit	10463523	9153799
Whatman	Rezist 30 / 5.0 PTFE	5.0 µm filter unit	10463533	G9966198
Fujifilm	DMC-11610	10 pL cartridge	2100201146	N/A
CH Instruments	Ag/AgCl reference electrode	Ref. electrode	CHI111	N/A

3.1.2 Ink preparation

Ink mixture is prepared by adding 1 wt. % carbon black with platinum and ruthenium into solvent base. Solvent base contains 10 wt. % Nafion (5 wt. % solution) and 90 wt. % diacetone alcohol (DAA)

The ink mixture was cooled, dispersed with homogenizer and magnetic stirred over-night. Finally, the ink was filtered through a 5 µm filter. A finer 1 µm filter was tried but rejected due to congestion.

3.1.3 Current collector preparation

11 cm x 11 cm x 125 µm PET substrate was cut and cleaned with isopropyl alcohol. Excess static charge of the substrate was removed with antistatic air blower in semi-clean room. The pattern mask and end-plate were cleaned and prepared as well. Substrate was sandwiched between the pattern mask and the end-plate. After preparation substrate is ready to be processed in vacuum evaporator.

In total five current collectors were produced. Alumina coated tungsten boat (~6.9 V) was used. Relative humidity was in 42–53 % range. Reasonable vacuum state (4.9–6.6 x 10^{-6} mbar) was achieved. Electrical current was gradually increased to 30 A to start evaporation process. The first 10 nm were evaporated to cover plate to prevent sub-

strate from contaminants, e.g. dust. Then the cover plate was removed and next 35 nm gold was evaporated directly to the substrate at rate of 0.2–0.3 Å/s. Finally, the cover plate was repositioned to prevent thicker formation of gold adhesion. Final vacuum pressure was in range of 5.0–9.9 x 10^{-5} mbar. Individual sample data is presented in appendix 3.

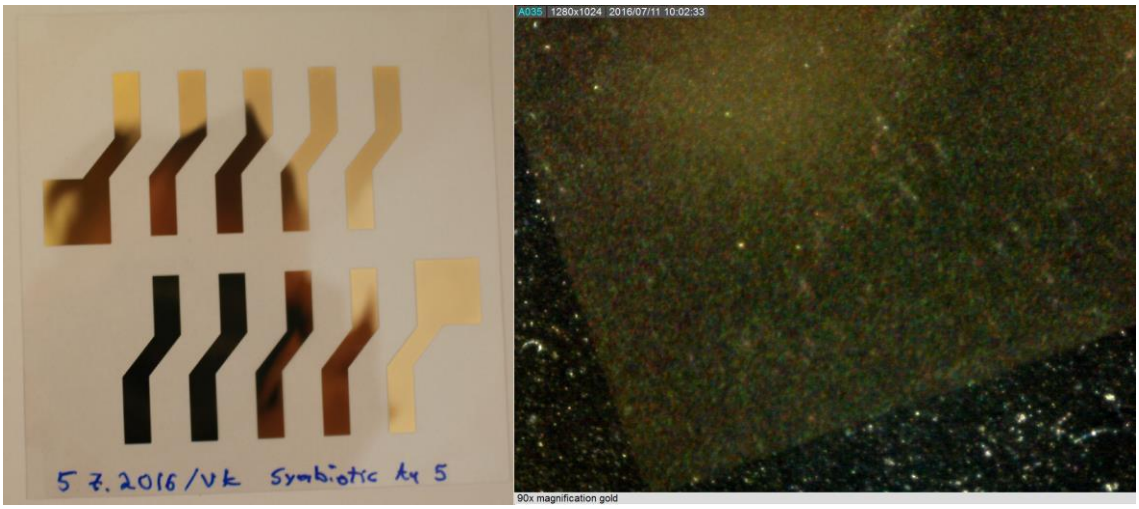

Figure 19. Photograph of current collector sample (left) and the gold surface of same sample (right) at 90x magnification (sample 5/5).

3.1.4 Electrode preparation

Carbon paper (Toray paper 060) and Nafion 117 were prepared in same fashion. Substrate was cut into approximately 20 cm x 5 cm sheet. Next the sheet was fixed to the PET support with adhesive tape. In total five layers of catalyst (Pt-Ru/C) were printed. In each layer an area of 2.5 cm x 2.5 cm was printed to the sample location. Five samples in total were printed on each substrate.

Cartridge used yields droplet volume of around 10 pL. Printing resolution was set to 1270 dpi (20 µm drop spacing) using 14 out of 16 jets (jets no. 3 to 16) with head angle set to 4.5°. Platen temperature was set to 30 °C. The print settings with more details are presented in appendix 4.

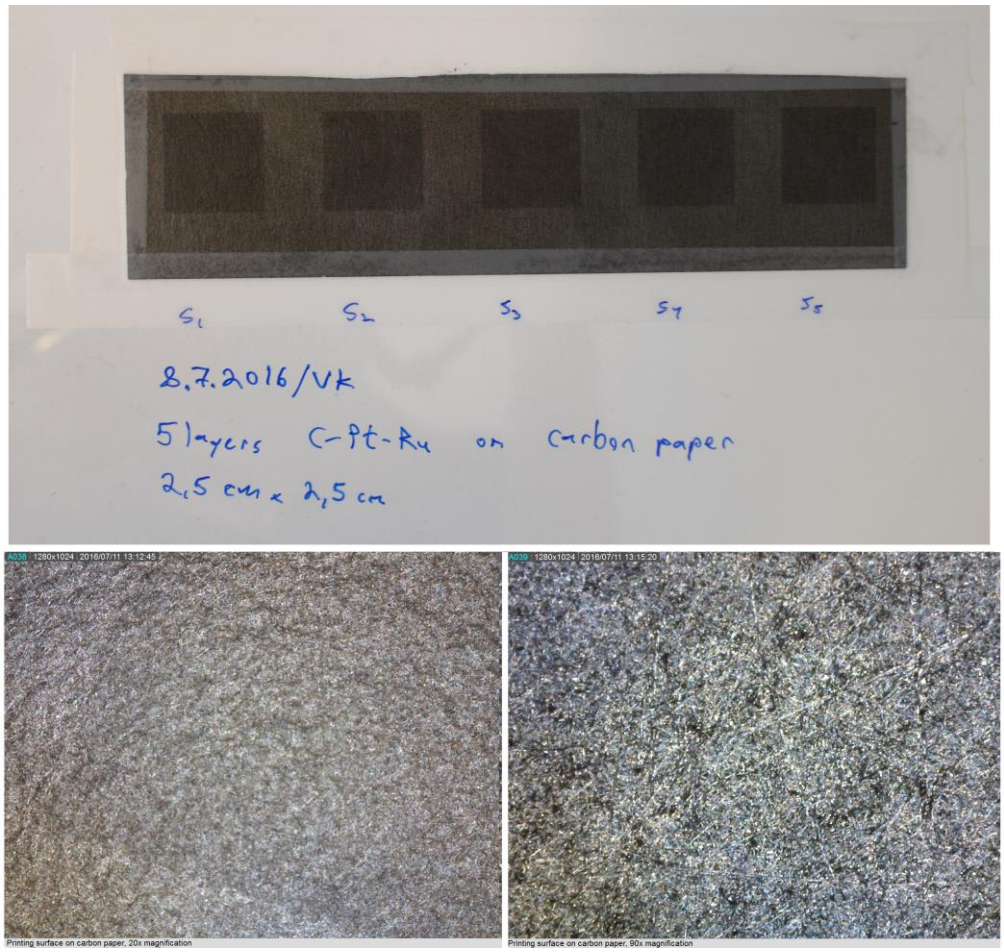

Figure 20. Carbon paper samples processed with C-Pt-Ru ink (top). Magnification of the sample no. 3 at 20x magnification (bottom left) and 90x magnification (bottom right).

Carbon paper was processed normally (Figure 20). Although same processing was applied to Nafion 117, the printing process for sheet of Nafion 117 was found to be problematic. Nafion sheet deformed due to wetting causing irregularities to the printing quality (i). The problem was solved by fixing the substrate more tightly to the platen by direct vacuum. This was achieved by making holes through the PET support sheet and superiorly sealing the holes to the substrate with adhesive tape. However final Nafion 117 samples (ii) were reprinted. See Figure 21.

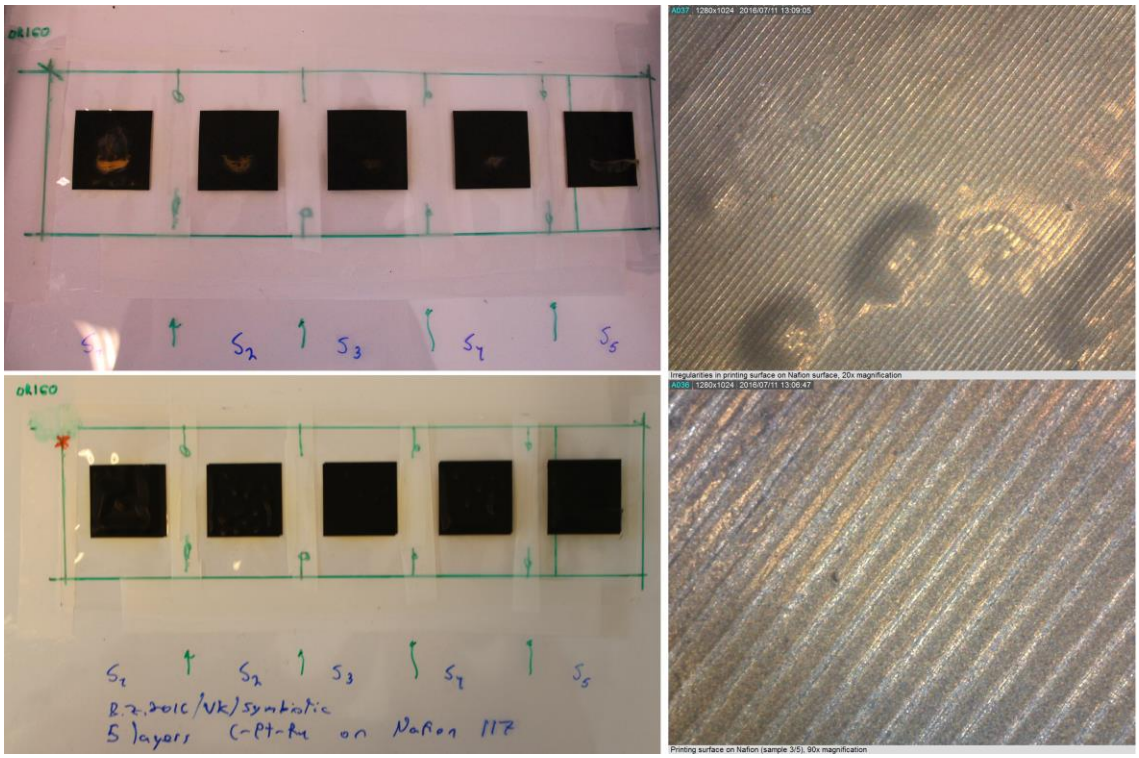

Figure 21. Nafion 117 samples processed with C-Pt-Ru ink. Printed Nafion samples before re-printing (top left), the irregularities in the printing pattern are shown. Final reprinted samples (bottom left) with smoother printing surface. Macroscopic deformation on surface is shown in the final sample no. 3 (top right) at 20x magnifications and the same sample surface is presented at 90x magnification (bottom right).

All samples were cut with scalpel from the sheet. Carbon paper samples were cut along the boundary of printing area (2.5 cm x 2.5 cm). Nafion samples were cut to square (3.5 cm x 3.5 cm) leaving 0.5 cm margin to the printing area. These Nafion prints were used for visual inspection only.

Additional two Nafion samples were printed in with same settings. The sample print size was 5 (9 mm distance) x 6 mm x 15 mm to match the current collector pattern. A sample with 10 layers and a sample with 20 layers were printed.

3.1.5 Cyclic voltammetry measurements

Active electrolyte solution (EA) with 0.5 M methanol (MeOH) and 0.5 M H_2SO_4 was prepared by measuring 3.8 g 99 % MeOH and 11.8 g H_2SO_4 and adding rest DIW to 240 mL. The solution was sonicated for 10 minutes and degassed another 10 minutes. Blank electrolyte (EB) solution was prepared in same fashion but leaving MeOH out.

Working electrodes were prepared by washing with DIW and sonicated in DIW for 10 minutes. Next they were polished with aluminium powder and washed with DIW and sonicated for 20 minutes in DIW. The electrodes were dried with nitrogen gas. Finally, two layers of sample ink were applied to the surface (8 µL + 8 µL) of the electrode. Each layer was given time to dry well before applying the second layer.

Active ink samples (A1, A2 and A3) were prepared by adding 7.5 mg Pt-Ru/C, 75 mg 5 wt. % Nafion perfluorinated resin solution and 675 mg DAA. Blank ink sample (B1, B2 and B3) were prepared same but adding 7.5 mg carbon black (Vulcan XC-72R) instead of Pt-Ru/C. All samples were dispersed for 30 minutes.

All samples were measured running 50 cycles using Iviumstat potentiostat. Reference electrode was Ag/AgCl (0.197 V vs. standard hydrogen electrode (SHE)) and auxiliary electrode was platinum. Graphite (disk geometry) electrodes were used as a working electrode. Measuring attributes were $E_i = E_{\lambda 2} = -0.2$ V and $E_{\lambda 1} = 1.0$ V. Scan rate was set to 50 mV/s, $E_{step} = 10$ mV, $\tau = 0.2$ s.

Measuring orders were A1EA, B3EA, B2EA, B1EA, A3EA, A2EA and A1EB, A3EB, B3EB, B2EB, B1EB, A2EB. All samples were reapplied and electrodes were cleaned and polished between the measurements of EA and EB. Numbers provided by random.org were used for randomization of the measuring order.

3.1.6 Cell assembly

Carbon paper GDL with 5 layers of Pt-Ru/C catalysts were carefully cut into ten 6 mm x 15 mm sheets. This forms cathode catalysts, the printing side is facing towards the Nafion membrane. Nafion with 20 layers Pt-Ru/C was used to form PEM and anode catalyst. Feeding and ventilation holes (8 holes per area) were punctured to the current collectors with 0.9 mm needle. See Figure 22 for schematics. All parts used are presented in Figure 23 and the completed assembly in Figure 24.

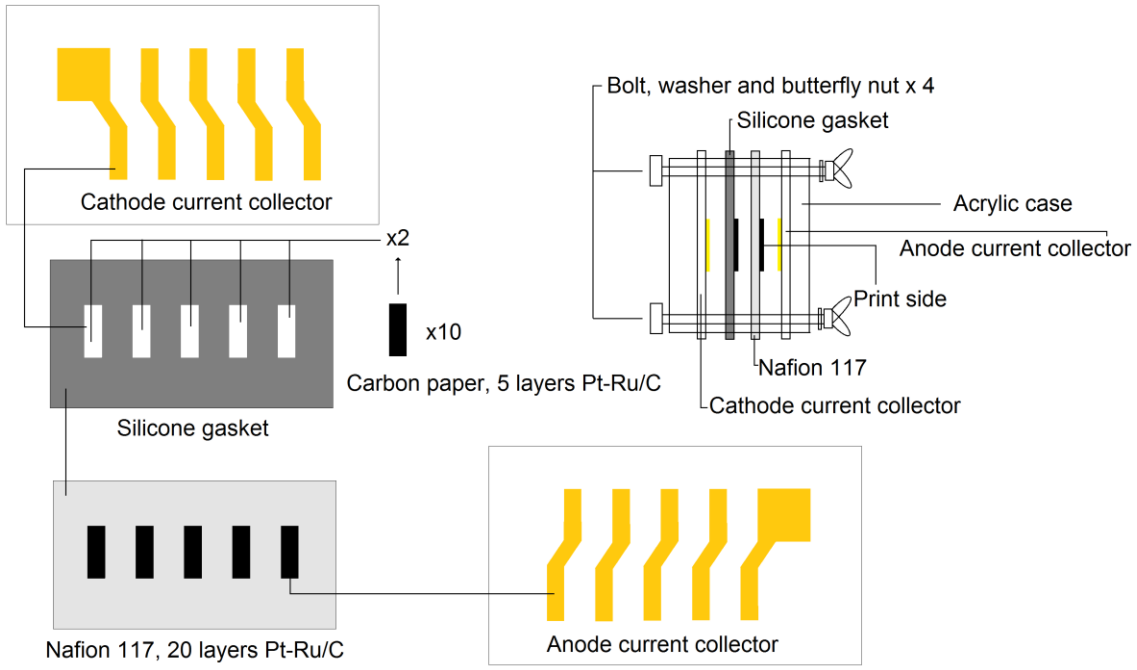

Figure 22.Schematics for prototype cell assembly

Figure 23. All parts ready before prototype cell assembly

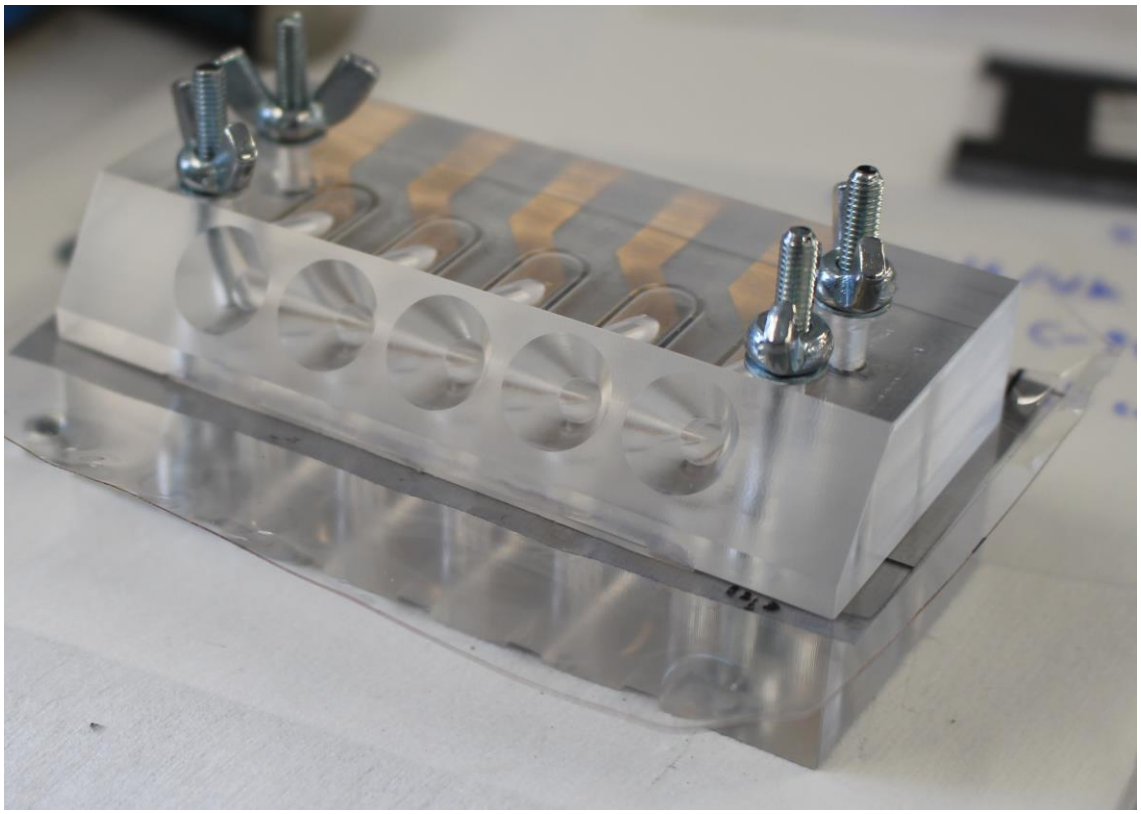

Figure 24. Assembled prototype direct methanol fuel cell in acrylic case with five individual methanol input ports for each MEA unit.

0.5 M MeOH and 0.5 H_2SO_4 in DIW injection (approx. 600 µL per MEA) was used as fuel. Electric potentials were measured for each individual MEA and in series to the complete DMFC. Bio-Logics SAS potentiostat was used for OCV measurements.

The second prototype was built using same construction but contained additional silicone gasket at anode between the anode current collector and Nafion print. Additionally, extra carbon paper sheets were added to anode to provide conductivity through the gasket opening.

4 Results

4.1 Cyclic voltammetry results for ink catalysis activity

Results were obtained by taking arithmetic mean of each sample quality for voltammetric cycles of 10, 20, 30, 40 and 50. Sample qualities were AEA (Pt-Ru/C ink with active electrolyte), AEB (Pt-Ru/C ink with blank electrolyte), BEA (Vulcan ink with active electrolyte) and BEB (Vulcan ink with blank electrolyte).

The highest current (9.3 mA) was exhibited by AEA at 0.78 V (1st scan phase, vs. sat. Ag/AgCl) in cycle no 50. AEB exhibited similar properties but lower current peak (4.5 mA) at 0.83 V (1st scan phase, vs. sat. Ag/AgCl). See Figure 25. Inactive Vulcan samples exhibited much lower reduction peaks both in EA and EB electrolytes compared to active Pt-Ru-C ink samples (see Figure 26).

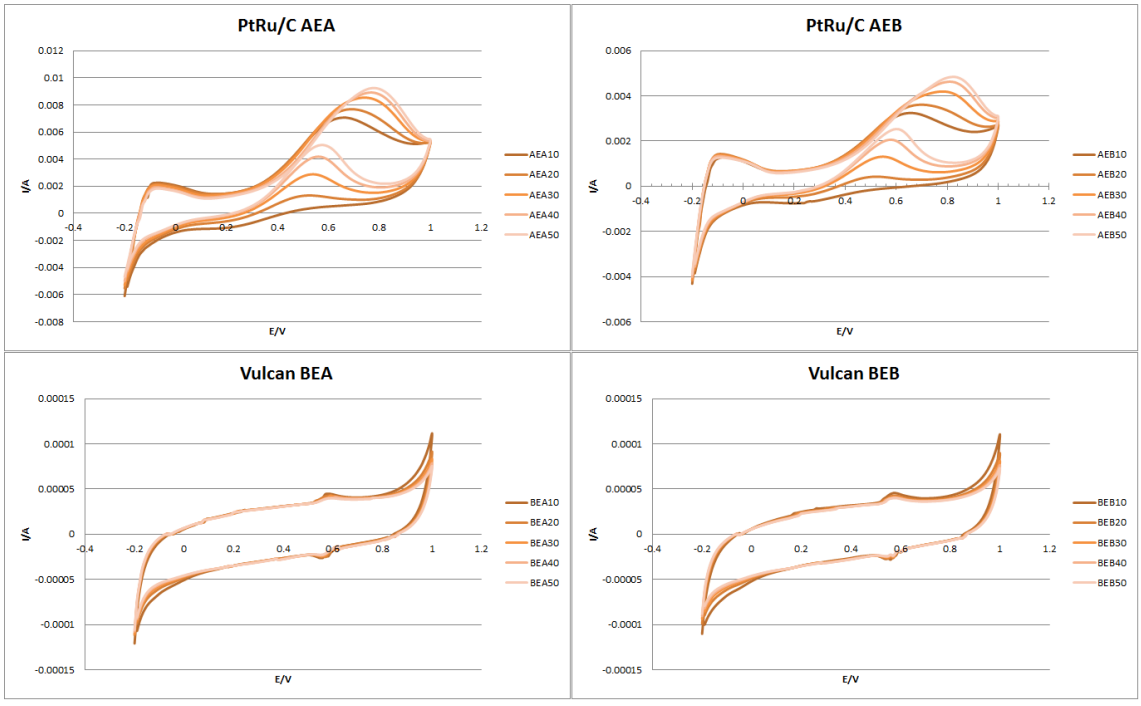

Figure 25. Cyclic voltammetry results, average of sample cycle no. 10, 20, 30, 40 and 50 per sample quality. Measured against saturated Ag/AgCl reference electrode.

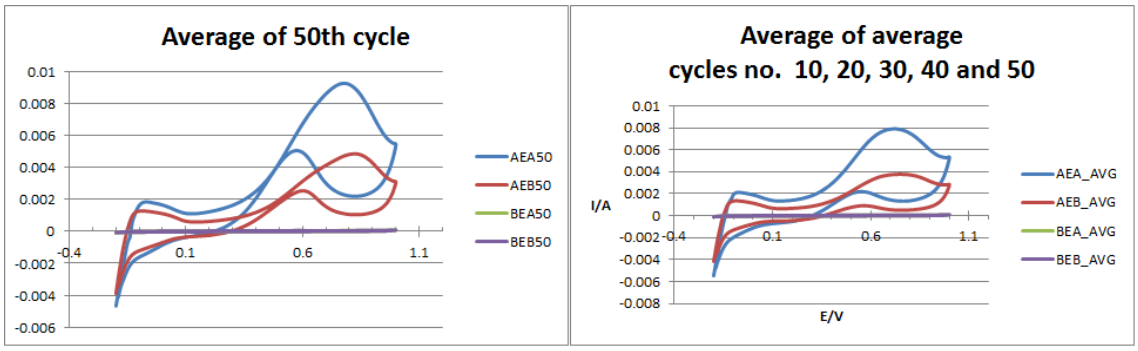

Figure 26.Average of 50th cycle per sample quality and average of cycles (no. 10, 20, 30, 40, 50) per sample quality. Measured against saturated Ag/AgCl reference electrode.

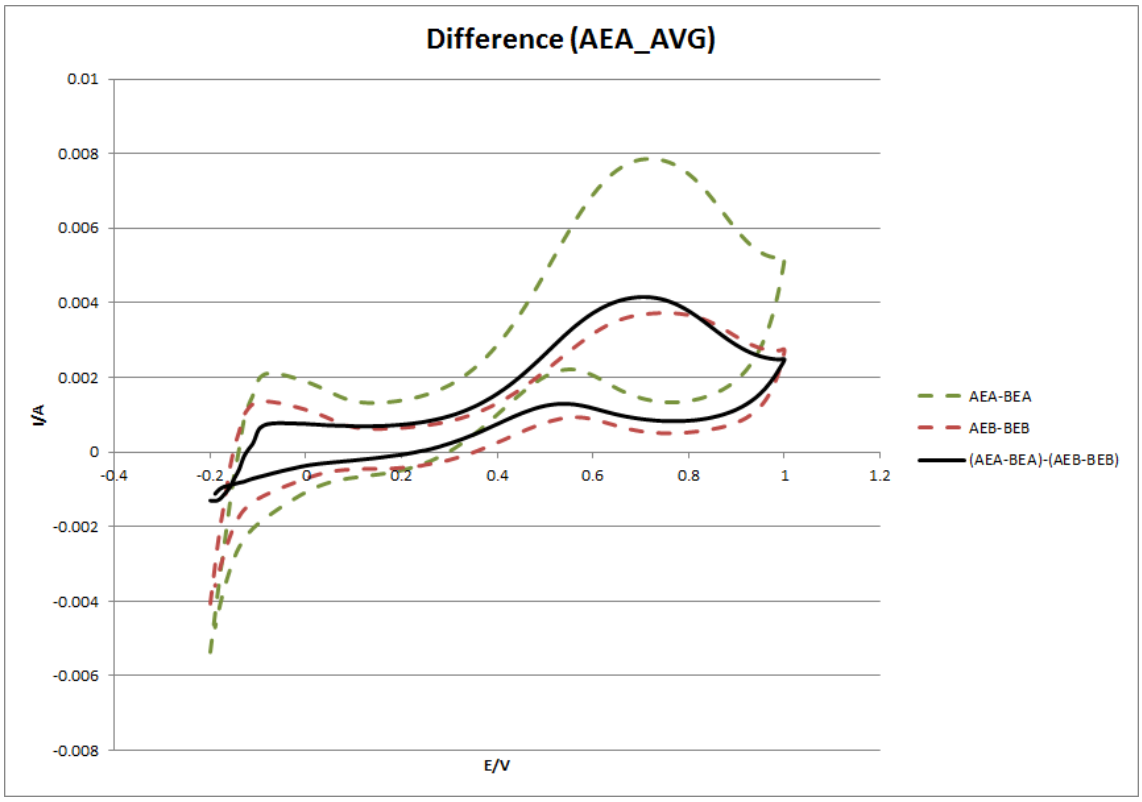

Figure 27.Difference of AEA_AVG compared to other sample average qualities. For example, AEA-BEA presents AEA_AVG where BEA_AVG is removed as background. Measured against saturated Ag/AgCl reference electrode

Average standard deviations in the sample qualities were 7.14 x 10^{-4}, 1.84 x 10^{-3}, 9.78 x 10^{-6} and 6.84 x 10^{-6} respectively to AEA, AEB, BEA, BEB. The highest standard deviation 2.29 x 10^{-3} between samples was found in samples A1EB50, A2EB50 and

A3EB50, AEB samples overall exhibited higher standard deviation compared to the other sample qualities.

4.2 Open-circuit voltage measurements for prototype DMFC assembly

Methanol was injected to the cells at 5 minutes (approx. 300 s). MEA1, MEA2, MEA3 and MEA4 exhibited no activity.

Only MEA5 presented some sort of electrical potential activity in the constructed DMFC prototype (see Figure 28). The adequate operation phase starts after 18 minutes of methanol injection, continuing 10 minutes (between 1400 s and 2000 s). The strongest potential peak (18.5 mV) observed at adequate operation phase is after 25 minutes of methanol injection (at 1824 s). The operation phase ends after approx. 28 minutes of methanol injection (at 2000 s).

Strong electric potential fluctuation starts at 40 minutes (MEA5) after methanol injection (at approx. 2700 s). MEA5 exhibited its peak voltage (18.7 mV) at strong fluctuation phase after 53 minutes (approx. 3180 s) of methanol injection and starts after that strongly fluctuating and decreasing to null. The activity ends after 235 minutes of methanol injection, not shown in Figure 28.

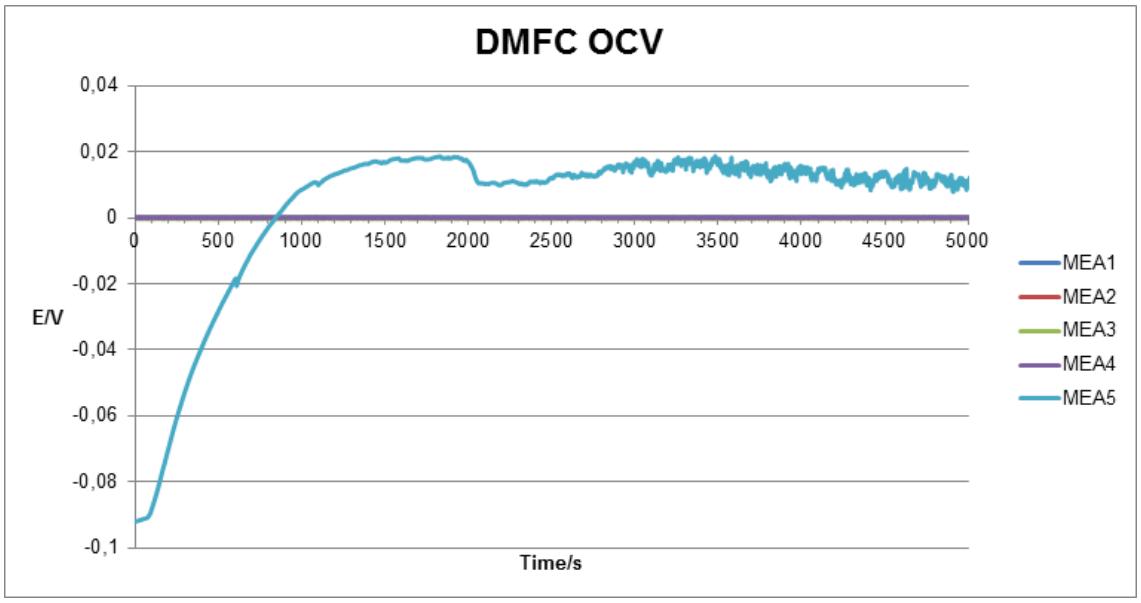

Figure 28. Measured open-circuit voltages per MEA in the first prototype DMFC.

5 Discussion

5.1 Pt-Ru/C loadings

Assuming complete distribution of Pt-Ru/C in ink, Pt-Ru/C catalyst loadings for substrates can be estimated per layer (Equation 5.1.1) and layered substrate, whereas *x* represents the number of layers (*N*) (Equation 5.1.2). Ink formulation yields approx. 100 pg Pt-Ru/C per droplet (10 pL). Print spacing was set to 20 µm. m_{PtRuC}/m_{ink} ratio 0.01 and the density of ink (ρ_{ink}) can be estimated to be 940 kg/m^3.

$$k_{LayerPtRuC} = \frac{m_{PtRuC} \times \rho_{ink} \times V_{droplet}}{A_{print\_area} \times m_{ink}} \approx 2.35 \times 10^{-4}\ \mathrm{kg\ m^{-2}} \quad (5.1.1)$$

$$m_{PtRuC} = A \times \int_0^N k_{LayerPtRuC}\, dx \quad (5.1.2)$$

Loadings of ink samples on electrodes (5 mm, disk) were 767 pg/cm^2 (2 layers, $V_{droplet}$ = 8.0 x 10^{-15} m^3, A_{print_area} = 7.85 x 10^{-6} m^2).

The total loadings in the Nafion print (10 and 20 layers, A_{print_area} = 4.0 x 10^{-10} m^2, $V_{droplet}$ = 1.0 x 10^{-14} m^3) can be estimated to be 235 µg/cm^2 and 470 µg/cm^2. Respectively, pure platinum loadings would be 0.07 mg/cm^2 and 0.14 mg/cm^2. Typical anode Pt-Ru/C loadings in PEMDMFCs presented in literature are 2–4 mg/cm^2, this would require 85 to 170 layers of printing. As low as 0.04 mg/cm^2 pure platinum loadings without carbon are used in low-power hydrogen fed fuel cells, however, in methanol fuel cells platinum-ruthenium is often preferred due to increased activity of active platinum binding sites. See Appendix 5 for calculation details.

5.2 Pt-Ru/C ink cyclic voltammetry measurements

A clear trend of increasing measured current as a function of cycles (time) in CV measurements of active Pt-Ru/C ink could be related to some kind of wetting issue due to nature of hydrophobic properties of Nafion. In the experiment situation, a visible

bubble was inspected between the electrode surface and electrolyte. This may partially be caused by the formation of carbon dioxide in methanol oxidation reaction. However, hydrophilic properties of Nafion in ink may additionally have their influence to the size of bubble or air pocket.

Reduction peak anomalies observed at 0.6 V (vs. sat. Ag/AgCl) with AEB samples could be related to possible interactions with Nafion[87] or to unknown contaminant, however, the reduction peaks observed on electrode were not as high compared to the AEA samples, which supports the increased oxidation of methanol. The measurement reliability of the methanol oxidation catalysis activity of Pt-Ru/C ink could potentially be improved by using different polymer instead of Nafion as fixing agent.

Overall, the results obtained support the Pt-Ru/C ink catalysis activity for methanol oxidation. However wetting issues with aqueous methanol can be problematic for a stable and quick function of direct methanol fuel cell. Potential solutions could be pre-wetting the anode surface before methanol solution is applied.

5.3 DMFC prototype open-circuit voltage measurements

In the prototype only MEA5 presented OCV activity. This can partially be explained that the prototype construction was not tight enough for optimal proton and electron conductivity. Additionally, some methanol spreading was detected, which may result to short circuit. Optimal MEA construction should be tightly packed to enable optimal proton conductivity between anode and cathode via PEM layer. Hot pressing technique could offer benefits to overcome the problem in operational functionality by strongly sandwiching the components together. Moreover, the catalyst layers could be bound more tightly to PEM by printing the both anode and cathode catalyst layers on opposite planes of the same PEM.

However, more research is needed. Other types of cell assemblies may offer better structures for controlled methanol flow.

The strong electric potential fluctuation that starts after 40 minutes of methanol injection could indicate to the methanol crossover, which would cause the mixed potential to anode and cathode.

Anode: $CH_3OH + H_2O \longrightarrow CO_2 + 6\,H^+ + 6\,e^-$ (5.3.1)

Cathode: $6\,H^+ + 6\,e^- + \frac{3}{2}\,O_2 \longrightarrow 3\,H_2O$ (5.3.2)

Cell: $CH_3OH + \frac{3}{2}\,O_2 \longrightarrow CO_2 + 2\,H_2O$ (5.3.3)

$$E° = \frac{\Delta G_{rxn}}{n_{electron} \times F} \quad (5.3.4)$$

$$\mu_f = \frac{E_{measured}}{E°} \quad (5.3.5)$$

Anode, cathode and overall net reaction in cell are presented in Equations 5.3.1–5.3.3. In the Equation 5.3.4 ΔG_{rxn} represents Gibbs free energy for a mole of methanol oxidation in DMFC (-702.07 kJ/mol), $n_{electrons}$ is the number of moles electrons transferred per mole of methanol (6 mol) and F is the faraday constant (96485 C/mol). Therefore, the standard electrode potential ($E°$) for methanol oxidation reaction is 1.2 V. ΔH_{rxn} is the standard heat of formation in combustion (higher heating value, HHV) reaction (Equation 5.3.6) for a mole of methanol with oxygen (-724.07 kJ/mol). See appendix 1.

$$2\,CH_3OH\,(l) + 3\,O_2\,(g) \longrightarrow 2\,CO_2\,(g) + 4\,H_2O\,(l) \quad (5.3.6)$$

$$\eta = \mu_f \times \frac{\Delta G_{rxn}}{\Delta H_{rxn}} = 0.015 \times \frac{-702.07 \times 10^{-3}\,J\,mol^{-1}}{-724.07 \times 10^{-3}\,J\,mol^{-1}} \approx 0.015 \quad (5.3.7)$$

Overall even MEA5 exhibited very low fuel coefficient (Equation 5.3.5) approx. 1.5 % based on its peak operational potential ($E_{measured}$ = 0.0185 V) and comparing it to the theoretical ideal OCV (1.2 V). This could be due to many reasons mentioned at the beginning of this chapter. However, many other reasons can be additionally related to this, for example the oxygen breathing rate or even the methanol adsorption rate to anode catalyst, which may be reduced due to hydrophilic properties of Nafion, which is included to the Pt-Ru/C ink as fixation agent due to polymeric properties. Additionally, same Pt-Ru/C ink was utilised to print cathode catalyst layer on carbon paper, typically in literature Pt/C is preferred. More research is needed to systematically answer these questions.

Overall the prototype DMFC MEA5 efficiency (Equation 5.3.7) was very low 1.5 % (HHV) and the total prototype fuel cell efficiency even lower. Virtually MEA1, MEA2, MEA3, MEA4 exhibiting null efficiency.

6 Conclusions

Pt-Ru/C ink exhibited higher reduction activity in active methanol electrolyte compared to the activity in inactive electrolyte, which supports the activity for methanol oxidation. However peak reduction anomalies presented in Pt-Ru/C in inactive electrolyte could be related to some interactions with Nafion itself, which may have affected the reduction peaks in active electrolyte as well. The reduction peaks of Pt-Ru/C ink in the active electrolyte are twice the amplitude compared to the reduction peaks in inactive electrolyte, which supports the increased methanol oxidation activity.

At current prototype stage the MEA construction is not reliable enough for adequate operational functionality. The overall exhibited efficiency is extremely low. More research is needed for optimal DMFC assembly using printed components, which would enable all its components work reliably together. Additionally, potential wetting issues with Nafion and methanol needs to be resolved.

Overall Inkjet printing technology can be used to produce functional passive direct methanol fuel cell. Additionally, inkjet printing reduces material waste due to well controlled printing. However, problems can arise at larger production quantities from the overall printing speed and the cost of printer parts compared to other production techniques.

References

1. Symbiotic. Symbiotic EU Project [Internet]. 2016 [cited 2016 May 30]. Available from: http://symbiotic-project.eu/project/

2. European Commission. Evaluation Summary Report - Research and innovation actions/Innovation actions. 2015.

3. Bohunicky B, Mousa SA. Biosensors: The new wave in cancer diagnosis. Nanotechnol. Sci. Appl. 2011;4:1–10.

4. Barbir F. PEM Fuel Cells: Theory and Practice. Pem Fuel Cells Theory Pract. Academic Press; 2005.

5. Pollet BG, Staffell I, Shang JL. Current status of hybrid, battery and fuel cell electric vehicles: From electrochemistry to market prospects. Electrochim. Acta [Internet]. Elsevier Ltd; 2012;84:235–49. Available from: http://dx.doi.org/10.1016/j.electacta.2012.03.172

6. Sharaf OZ, Orhan MF. An overview of fuel cell technology: Fundamentals and applications. Renew. Sustain. Energy Rev. [Internet]. Elsevier; 2014;32:810–53. Available from: http://dx.doi.org/10.1016/j.rser.2014.01.012

7. European Commission. Horizon 2020 Call: H2020-FETOPEN-2014-2015-RIA. European Comission; 2014.

8. Li Y, Yang HH, You QH, Zhuang ZX, Wang XR. Protein recognition via surface molecularly imprinted polymer nanowires. Anal. Chem. 2006;78:317–20.

9. Moreira FTC, Sharma S, Dutra RAF, Noronha JPC, Cass AEG, Sales MGF. Smart plastic antibody material (SPAM) tailored on disposable screen printed electrodes for protein recognition: Application to myoglobin detection. Biosens. Bioelectron. 2013;45:237–44.

10. Renkema JMS, Gruppen H, Van Vliet T. Influence of pH and ionic strength on heat-induced formation and rheological properties of soy protein gels in relation to denaturation and their protein compositions. J. Agric. Food Chem. 2002;50:6064–71.

11. Greiner W, Müller B. Gauge Theory of Weak Interactions [Internet]. Gauge Theory Weak Interact. Berlin, Heidelberg: Springer Berlin Heidelberg; 2009 [cited 2016 Jun 9]. Available from: http://link.springer.com/10.1007/978-3-662-03323-4_1

12. Strassler M. The Strengths of the Known Forces | Of Particular Significance [Internet]. [cited 2016 Jun 9]. Available from: https://profmattstrassler.com/articles-and-posts/particle-physics-basics/the-known-forces-of-nature/the-strength-of-the-known-forces/

13. Srinivasan K, Gu J. Lightning as atmospheric electricity. Can. Conf. Electr. Comput. Eng. 2007;2258–61.

14. Larminie J, Dicks A. Fuel Cell Systems Explained. Second. J. Power Sources. West Sussex, England: Wiley; 2003.

15. Mabbott GA. An introduction to cyclic voltammetry. J. Chem. Educ. [Internet]. 1983;60:697–702. Available from: http://dx.doi.org/10.1021/ed060p697

16. Bacher A, Rezai S. Cyclic Voltammetry [Internet]. 2003 [cited 2016 Aug 1]. Available from: http://www.chem.ucla.edu/~bacher/CHEM174/equipment/CV1.html

17. Runnels PL, Joseph JD, Logman MJ, Wightman RM. Effect of pH and surface functionalities on the cyclic voltammetric responses of carbon-fiber microelectrodes. Anal. Chem. 1999;71:2782–9.

18. Kirubakaran A, Jain S, Nema RK. A review on fuel cell technologies and power electronic interface. Renew. Sustain. Energy Rev. 2009;13:2430–40.

19. Fedkin M. 10.2. Zero Emission Vehicles [Internet]. The Pennsylvanian State University; 2015 [cited 2016 May 27]. Available from: https://www.e-education.psu.edu/eme807/node/671

20. Wang L, Mao H, Zhou X, Xu Q, Li Q. The Impregnating Reduction Method for Synthesis of Pt–Ru Nanoparticles and Its Catalytic Performance for Methanol Electro-oxidation. J. Fuel Cell Sci. Technol. [Internet]. 2015;12:041001. Available from: http://fuelcellscience.asmedigitalcollection.asme.org/article.aspx?doi=10.1115/1.4029874

21. Guo Z, Cao Y. A passive fuel delivery system for portable direct methanol fuel cells. J. Power Sources. 2004;132:86–91.

22. Tuurala S. Characterization of PEM Fuel Cell Porous Transport Layers. Helsinki University of Technology; 2008.

23. Litster S, McLean G. PEM fuel cell electrodes. J. Power Sources. 2004;130:61–76.

24. EG&G Technical Services Inc. Fuel Cell Handbook [Internet]. Fuel Cell. 2004. Available from: http://www.osti.gov/energycitations/product.biblio.jsp?osti_id=5616450

25. Merle G, Wessling M, Nijmeijer K. Anion exchange membranes for alkaline fuel cells: A review. J. Memb. Sci. 2011;377:1–35.

26. Ormerod RM. Solid oxide fuel cells. Chem. Soc. Rev. [Internet]. 2003;32:17–28. Available from: http://xlink.rsc.org/?DOI=b105764m

27. Steele BC, Heinzel A. Materials for fuel-cell technologies. Nature. 2001;414:345–52.

28. Leech D, Kavanagh P, Schuhmann W. Enzymatic fuel cells: Recent progress. Electrochim. Acta [Internet]. Elsevier Ltd; 2012;84:223–34. Available from:

http://dx.doi.org/10.1016/j.electacta.2012.02.087

29. Ferri S, Kojima K, Sode K. Review of glucose oxidases and glucose dehydrogenases: a bird's eye view of glucose sensing enzymes. J. Diabetes Sci. Technol. [Internet]. 2011;5:1068–76. Available from: http://www.pubmedcentral.nih.gov/articlerender.fcgi?artid=3208862&tool=pmcentrez&rendertype=abstract

30. Walker AL, Walker CW. Biological fuel cell and an application as a reserve power source. J. Power Sources. 2006;160:123–9.

31. Atamna H, Nguyen A, Schultz C, Boyle K, Newberry J, Kato H, et al. Methylene blue delays cellular senescence and enhances key mitochondrial biochemical pathways. FASEB J. 2008;22:703–12.

32. Lodish H, Berk A, Zipursky SL, Matsudaira P, Baltimore D, Darnell J. Oxidation of Glucose and Fatty Acids to CO2. Mol. Cell Biol. New York: W. H. Freeman; 2000.

33. Rawson FJ, Downard AJ, Baronian KH. Electrochemical detection of intracellular and cell membrane redox systems in Saccharomyces cerevisiae. Sci. Rep. [Internet]. The Author(s); 2014;4:5216. Available from: http://dx.doi.org/10.1038/srep05216

34. Kim HJ, Park HS, Hyun MS, Chang IS, Kim M, Kim BH. A mediator-less microbial fuel cell using a metal reducing bacterium, Shewanella putrefaciens. Enzyme Microb. Technol. 2002;30:145–52.

35. Adamson KA, Pearson P. Hydrogen and methanol: A comparison of safety, economics, efficiencies and emissions. J. Power Sources. 2000;86:548–55.

36. Lucia U. Overview on fuel cells. Renew. Sustain. Energy Rev. [Internet]. Elsevier; 2014;30:164–9. Available from: http://dx.doi.org/10.1016/j.rser.2013.09.025

37. Li X, Faghri A. Review and advances of direct methanol fuel cells (DMFCs) part I: Design, fabrication, and testing with high concentration methanol solutions. J. Power Sources [Internet]. Elsevier B.V; 2013;226:223–40. Available from: http://dx.doi.org/10.1016/j.jpowsour.2012.10.061

38. Li Q, He R, Gao J-A, Jensen JO, Bjerrum NJ. The CO Poisoning Effect in PEMFCs Operational at Temperatures up to 200°C. J. Electrochem. Soc. [Internet]. 2003;150:A1599–605. Available from: http://jes.ecsdl.org/content/150/12/A1599.abstract

39. Janssen GJM, Lebedeva NP. Carbon dioxide poisoning on proton-exchange-membrane fuel cell anodes. Sci. Technol. 2005. p. 6–7.

40. Igarashi H, Fujino T, Watanabe M. Hydrogen electro-oxidation on platinum catalysts in the presence of trace carbon monoxide. J. Electroanal. Chem. 1995;391:119–23.

41. Baschuk JJ, Li X. Carbon monoxide poisoning of proton exchange membrane fuel cells. Int. J. Energy Res. 2001;25:695–713.

42. Shakhashiri B. Gases of the air. 2007; Available from: www.scifun.org

43. DuPont. DuPont Fuel Cells - Membrane Electrode Assemblies. Data Sheet. 2009;1–2.

44. Fuel Cell Store. Membrane Electrode Assemblies (MEA) [Internet]. 2016 [cited 2016 Jun 2]. Available from: http://fuelcellstore.com/fuel-cell-components/membrane-electrode-assembly

45. Zhang J, Yin GP, Lai QZ, Wang ZB, Cai K Di, Liu P. The influence of anode gas diffusion layer on the performance of low-temperature DMFC. J. Power Sources. 2007;168:453–8.

46. Hickner MA, Ghassemi H, Kim YS, Einsla BR, McGrath JE. Alternative polymer systems for proton exchange membranes (PEMs). Chem. Rev. 2004;104:4587–611.

47. Lufrano F, Squadrito G, Patti A, Passalacqua E. Sulfonated polysulfone as promising membranes for polymer electrolyte fuel cells. J. Appl. Polym. Sci. 2000;77:1250–6.

48. Sigma-Aldrich. Safety Data Sheet: Nafion® perfluorinated membrane. Sigma-Aldrich; 2015.

49. Sigma-Aldrich. Nafion® perfluorinated membrane [Internet]. Online Cat. 2016 [cited 2016 May 26]. Available from: http://www.sigmaaldrich.com/catalog/product/aldrich/541346

50. Yakovlev S, Balsara NP, Downing KH. Insights on the study of nafion nanoscale morphology by transmission electron microscopy. Membranes (Basel). 2013;3:424–39.

51. FuelCellsEtc. Nafion 115 [Internet]. Online Cat. 2016 [cited 2016 Jun 8]. Available from: http://fuelcellsetc.com/store/N115?search=nafion

52. Woo Y, Oh SY, Kang YS, Jung B. Synthesis and characterization of sulfonated polyimide membranes for direct methanol fuel cell. J. Memb. Sci. 2003;220:31–45.

53. Pintauro PN, Wycisk R. Polymeric Membranes for Fuel Cells: Overview and Future Outlook. Cleveland: Case Western Reserve University;

54. Silva RF, De Francesco M, Pozio A. Solution-cast Nafion?? ionomer membranes: Preparation and characterization. Electrochim. Acta. 2004;49:3211–9.

55. Tang Y, Yuan W, Pan M, Tang B, Li Z, Wan Z. Effects of structural aspects on the performance of a passive air-breathing direct methanol fuel cell. J. Power Sources [Internet]. Elsevier B.V.; 2010;195:5628–36. Available from: http://dx.doi.org/10.1016/j.jpowsour.2010.03.069

56. Liu JG, Zhao TS, Liang ZX, Chen R. Effect of membrane thickness on the

performance and efficiency of passive direct methanol fuel cells. J. Power Sources. 2006;153:61–7.

57. Apanel G, Johnson E. Direct methanol fuel cells - Ready to go commercial? Fuel Cells Bull. 2004;2004:12–7.

58. Bernfeld GJ, Bird AJ, Edwards RI, Köpf H, Köpf-Maier P, Raub CJ, et al. Platinum-Group Metals, Alloys and Compounds in Catalysis. Pt Platin. [Internet]. Berlin, Heidelberg: Springer Berlin Heidelberg; 1985 [cited 2016 Jun 9]. p. 92–317. Available from: http://link.springer.com/10.1007/978-3-662-10278-7_4

59. Sobrova P, Zehnalek J, Adam V, Beklova M, Kizek R. The effects on soil/water/plant/animal systems by platinum group elements. Cent. Eur. J. Chem. [Internet]. 2012;10:1369–82. Available from: http://www.springerlink.com/index/10.2478/s11532-012-0073-7

60. Baghalha M, Khosravian Gh. H, Mortaheb HR. Kinetics of platinum extraction from spent reforming catalysts in aqua-regia solutions. Hydrometallurgy [Internet]. Elsevier B.V.; 2009;95:247–53. Available from: http://dx.doi.org/10.1016/j.hydromet.2008.06.003

61. Hamnett A. Mechanism and electrocatalysis in the direct methanol fuel cell. Catal. Today [Internet]. 1997;38:445–57. Available from: http://www.sciencedirect.com/science/article/pii/S0920586197000540

62. Iwasita T. Electrocatalysis of methanol oxidation. Electrochim. Acta. 2002;47:3663–74.

63. Waszczuk P, Lu GQ, Wieckowski A, Lu C, Rice C, Masel RI. UHV and electrochemical studies of CO and methanol adsorbed at platinum/ruthenium surfaces, and reference to fuel cell catalysis. Electrochim. Acta. 2002;47:3637–52.

64. Ge J, Higier A, Liu H. Effect of gas diffusion layer compression on PEM fuel cell performance. J. Power Sources. 2006;159:922–7.

65. Donnet J-B, Bansal RC, Wang M-J. Carbon black : science and technology. Dekker; 1993.

66. Niyogi S, Bekyarova E, Itkis ME, Mcwilliams JL, Hamon MA, Haddon RC. Solution Properties of Graphite and Graphene. J. Am. Chem. Soc. 2006;128:7720–1.

67. Insepov Z, Wolf D, Hassanein A. Nanopumping using carbon nanotubes. Nano Lett. 2006;6:1893–5.

68. Thostenson ET, Ren Z, Chou T-W. Advances in the science and technology of carbon nanotubes and their composites: a review. Compos. Sci. Technol. 2001;61:1899–912.

69. Yang Q, Li F, Hou P, Liu C, Liu M, Cheng H. Evaluation of diameter distribution of

inside cavities of open CNTs by analyses of nitrogen cryo-adsorption isotherm. Chinese Sci. Bull. [Internet]. 2001;46. Available from: http://link.springer.com/article/10.1007/BF03184334

70. Bruce DW, O'Hare D, Walton RI, editors. Porous Materials [Internet]. Chichester, UK: John Wiley & Sons, Ltd; 2010. Available from: http://doi.wiley.com/10.1002/9780470711385

71. De Volder MFL, Tawfick SH, Baughman RH, Hart AJ. Carbon nanotubes: Present and future commercial applications. Science (80-.). [Internet]. 2013;339:535–9. Available from: http://www.scopus.com/inward/record.url?eid=2-s2.0-84873808704&partnerID=40&md5=d3f25d18ac1d028575d64a46e9fba478

72. Fuelcellsetc. What is the Difference Between Carbon Paper and Carbon Cloth Based Gas Diffusion Layers (GDL)? [Internet]. 2013 [cited 2016 Jul 14]. Available from: http://fuelcellsetc.com/2013/03/comparing-gas-diffusion-layers-gdl/

73. Zamel N, Li X, Shen J, Becker J, Wiegmann A. Estimating effective thermal conductivity in carbon paper diffusion media. Chem. Eng. Sci. 2010;65:3994–4006.

74. Gooden K, Laudari A, Knotts G, Guha S. Printed dielectric-based organic diodes and transistors. Flex. Print. Electron. [Internet]. IOP Publishing; 2016;1:015004. Available from: http://stacks.iop.org/2058-8585/1/i=1/a=015004?key=crossref.2eb5235d51e78012b2c9a1753b51442b

75. Meissner M V, Spengler N, Mager D, Wang N, Kiss SZ, Höfflin J, et al. Ink-jet printing technology enables self-aligned mould patterning for electroplating in a single step. J. Micromechanics Microengineering [Internet]. IOP Publishing; 2015;25:65015. Available from: http://stacks.iop.org/0960-1317/25/i=6/a=065015

76. Singh M, Haverinen HM, Dhagat P, Jabbour GE. Inkjet printing-process and its applications. Adv. Mater. 2010;22:673–85.

77. De Gans BJ, Kazancioglu E, Meyer W, Schubert US. Ink-jet Printing Polymers and Polymer Libraries Using Micropipettes. Macromol. Rapid Commun. 2004;25:292–6.

78. Le HP. Progress and trends in ink-jet printing technology. J. Imaging Sci. Technol. 1998;42:49–62.

79. Tekin E, Smith PJ, Schubert US. Inkjet printing as a deposition and patterning tool for polymers and inorganic particles. Soft Matter. 2008;4:703.

80. Nave CR. Reflection of Waves [Internet]. HyperPhysics. [cited 2016 Jul 1]. Available from: http://hyperphysics.phy-astr.gsu.edu/hbase/sound/reflec.html

81. Li X, Prof S. Ink-Jet Patterning of Functional Materials State of the Art and Prospect Name : Topmaster Nanosci. 2008;

82. Falcão DS, Pereira JP, Rangel CM, Pinto AMFR. Development and performance

analysis of a metallic passive micro-direct methanol fuel cell for portable applications. Int. J. Hydrogen Energy. 2014;0.

83. Barbera O, Stassi A, Sebastian D, Bonde JL, Giacoppo G. Simple and functional direct methanol fuel cell stack designs for application in portable and auxiliary power units. 2016;2–11.

84. Yan XH, Wu R, Xu JB, Luo Z, Zhao TS. A monolayer graphene - Nafion sandwich membrane for direct methanol fuel cells. J. Power Sources. 2016;311:188–94.

85. Yang Y, Liang YC. A direct methanol fuel cell system with passive fuel delivery based on liquid surface tension. J. Power Sources. 2007;165:185–95.

86. Hirano S, Kim J, Srinivasan S. High performance proton exchange membrane fuel cells with sputter-deposited Pt layer electrodes. Electrochim. Acta. 1997;42:1587–93.

87. Sleightholme AES, Kucernak A. An anomalous peak observed in the electrochemistry of the platinum/perfluorosulfonic acid membrane interface. Electrochim. Acta [Internet]. Elsevier Ltd; 2011;56:4396–402. Available from: http://dx.doi.org/10.1016/j.electacta.2010.12.036

Standard heats and free energies of formation and absolute entropies

Compound	State	ΔH(f°) (kJ/mol)	ΔG(f°) (kJ/mol)	S° (J/(deg*mol))	C(p°) (J/(deg*mol))
Methanol	liquid	-239,1	-166,6	126,8	81,2
Methanol	gas	-201	-162,3	239,9	44,1
Carbon monoxide	gas	-110,53	-137,16	197,66	29,14
Carbon dioxide	gas	-391,51	-394,39	213,785	37,13
Dioxygen	gas	0	0	205,152	29,4
Water	solid	-292,72			37,11
Water	liquid	-285,83	-237,14	69,95	75,35
Water	gas	-241,826	-228,61	188,853	33,6
Dihydrogen (H2)	gas	0	0	130,68	28,84
Hydrogen (H)	gas	217,998	203,3	114,717	20,8
Proton (H+)	aqueous	0	0	0	0

References N. Lange, Handbook of Chemistry. 1999

Certificate of analysis: C-30/15-Platinum/Ruthenium

Certificate of Analysis

Product Number:	43990
Product:	Platinum, nominally 30 %, Ruthenium nominally 15 % on carbon black
Lot no:	023239

Platinum	29.73 %
Ruthenium	15.01 %
Moisture	0.26 %
Platinum atomic	50.64 %
Ruthenium atomic	49.36 %
Hydrolyzable chloride	106 ppm
XRD Crystallite size	2.25 nm
Total Ca+Co+Cr+Cu+Fe+Mg+Ni+Pb	208 ppm

This document has been electronically generated and does not require a signature.

Notes from gold evaporation procedure

Date	Name	Material (Au)	Lot#	Substrate	p_min (mbar)	p_max (mbar)	RH-%	d (nm)	Rate (Å/s)	~I (A)
27.6.2016	Symbiotic Au 1	G4-5005-M	W41015-6	PET 125 µm	6,6E-06	9,9E-05	53	35	0,2-0,3	30
28.6.2016	Symbiotic Au 2	G4-5005-M	W41015-6	PET 125 µm	5,4E-06	6,3E-05	50	35	0,2-0,3	30
29.6.2016	Symbiotic Au 3	G4-5005-M	W41015-6	PET 125 µm	5,3E-06	5,6E-05	52	35	0,2-0,3	30
1.7.2016	Symbiotic Au 4	G4-5005-M	W41015-6	PET 125 µm	5,4E-06	5,4E-05	45	35	0,2-0,3	30
5.7.2016	Symbiotic Au 5	G4-5005-M	W41015-6	PET 125 µm	4,9E-06	5,0E-05	42	35	0,2-0,3	30

EU Symbiotic / Current collector (Au)

Vesa Koiramäki

5.7.2016

Settings for C-Pt-Ru ink in inkjet printing

Cartbridge settings

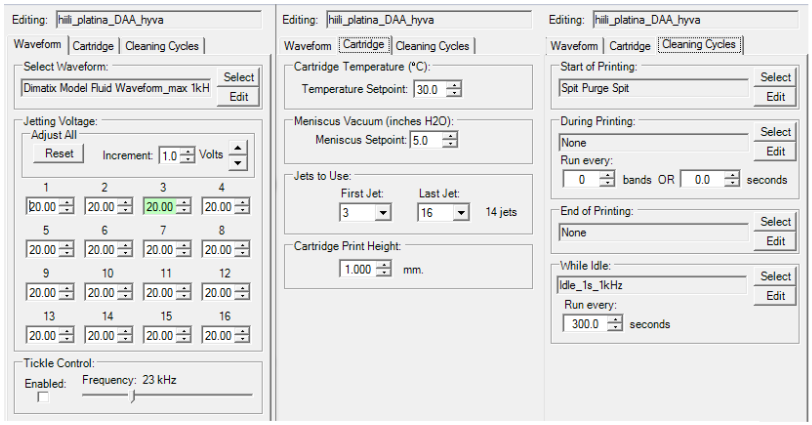

Pattern image

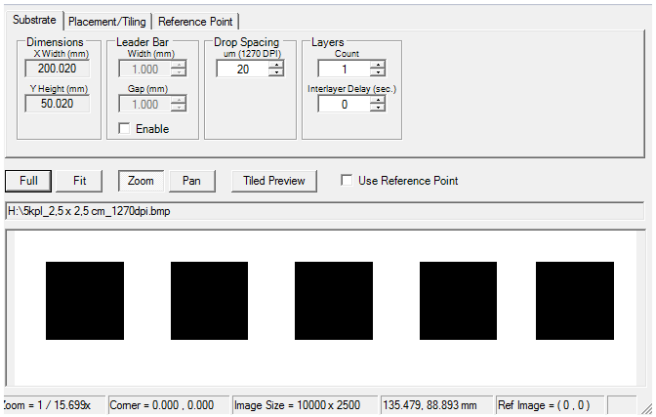

Split Purge Split

Idle_1s_1kHz

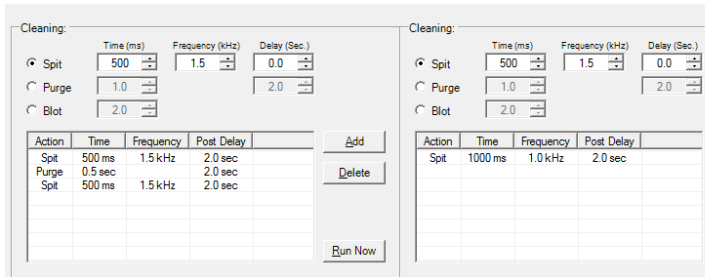

Jetting waveform

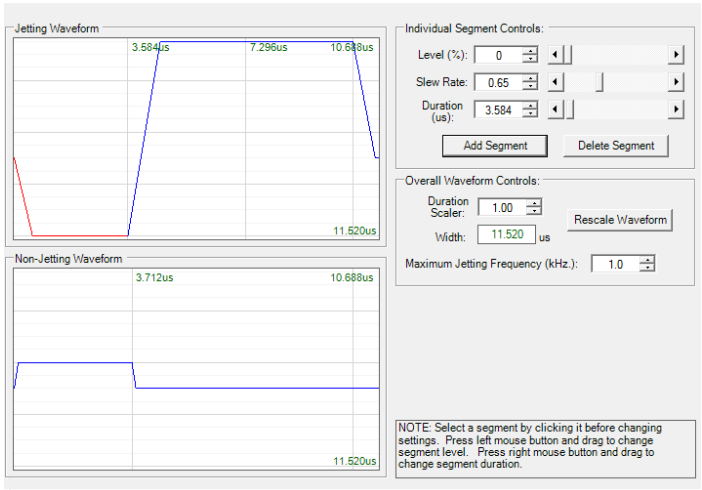

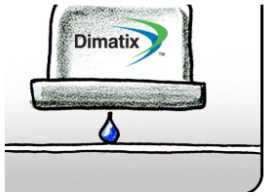

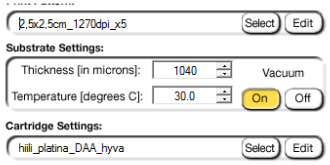

Calculation details

Calculations for hydrogen fuel cell ($2\ H_2\ (g) + 0_2\ (g) \longrightarrow 2\ H_2O$; $2\ H_2 \longrightarrow 4\ H^+ + 4\ e^-$)

Quantity	Dihydrogen(g)	Dioxygen (g)	Water (l)	Water (g)
dG(f)	0	0	-237,14	-228,61
dH(f)	0	0	-285,83	-241,826
n_l	2	1	2	0
n_g	2	1	0	2
n_l x dG(f)	0	0	-474,28	0
n_g x dG(f)	0	0	0	-457,22
n_l x dH(f)	0	0	-571,66	0
n_g x dG(f)	0	0	0	-483,652

dG(rxn_l)	-474,28	kJ	-474280	J
dG(rxn_g)	-457,22	kJ	-457220	J
dH(rxn_l)	-571,66	kJ	-571660	J
dH(rxn_g)	-483,652	kJ	-483652	J
Voltage_l	0,001228896	kV	1,22889568	V
Voltage_g	0,001184692	kV	1,18469192	V
Efficiency HHV	0,82965399		82,965399	%
Efficiency LHV	0,945349135		94,5349135	%

Calculations for estimated Pt-Ru/C loadings

Substance	Density (kg/m^3)	INK	Wt. %	Pt-Ru/C	
Nafion	874	Pt-Ru/C	1 %	Pt	0,2973
DAA	938	Nafion	10 %	Ru	0,1501
DAA/Naf (est)	931,6	Diacetone alcohol	90 %	C	0,8528
Ink (est.)	940,916				

Substance	Volume (m^3)	Drying area (m^2)	Mass (kg)	Pt-Ru/C (kg)
Droplet (10 pL)	1,00E-14	4,00E-10	9,41E-12	9,41E-14

Number of layers	Pt-Ru/C (kg)	Pt-Ru/C (mg)	A (m^2)	A (cm^2)	kg/m^2	mg/cm^2
1	9,41E-14	9,41E-08	4,00E-10	4,00E-06	2,35E-04	2,35E-02
5	4,70E-13	4,70E-07	4,00E-10	4,00E-06	1,18E-03	1,18E-01
10	9,41E-13	9,41E-07	4,00E-10	4,00E-06	2,35E-03	2,35E-01
20	1,88E-12	1,88E-06	4,00E-10	4,00E-06	4,70E-03	4,70E-01
100	9,41E-12	9,41E-06	4,00E-10	4,00E-06	2,35E-02	2,35E+00

Conversions	
1,00E+06	mg/kg
1,00E+04	cm^2/m^2

IUPAC Periodic Table of the Elements

1																	18
1 H hydrogen [1.007, 1.009]	2		Key: atomic number **Symbol** name standard atomic weight									13	14	15	16	17	2 He helium 4.003
3 Li lithium [6.938, 6.997]	4 Be beryllium 9.012											5 B boron [10.80, 10.83]	6 C carbon [12.00, 12.02]	7 N nitrogen [14.00, 14.01]	8 O oxygen [15.99, 16.00]	9 F fluorine 19.00	10 Ne neon 20.18
11 Na sodium 22.99	12 Mg magnesium [24.30, 24.31]	3	4	5	6	7	8	9	10	11	12	13 Al aluminium 26.98	14 Si silicon [28.08, 28.09]	15 P phosphorus 30.97	16 S sulfur [32.05, 32.08]	17 Cl chlorine [35.44, 35.46]	18 Ar argon 39.95
19 K potassium 39.10	20 Ca calcium 40.08	21 Sc scandium 44.96	22 Ti titanium 47.87	23 V vanadium 50.94	24 Cr chromium 52.00	25 Mn manganese 54.94	26 Fe iron 55.85	27 Co cobalt 58.93	28 Ni nickel 58.69	29 Cu copper 63.55	30 Zn zinc 65.38(2)	31 Ga gallium 69.72	32 Ge germanium 72.63	33 As arsenic 74.92	34 Se selenium 78.97	35 Br bromine [79.90, 79.91]	36 Kr krypton 83.80
37 Rb rubidium 85.47	38 Sr strontium 87.62	39 Y yttrium 88.91	40 Zr zirconium 91.22	41 Nb niobium 92.91	42 Mo molybdenum 95.95	43 Tc technetium	44 Ru ruthenium 101.1	45 Rh rhodium 102.9	46 Pd palladium 106.4	47 Ag silver 107.9	48 Cd cadmium 112.4	49 In indium 114.8	50 Sn tin 118.7	51 Sb antimony 121.8	52 Te tellurium 127.6	53 I iodine 126.9	54 Xe xenon 131.3
55 Cs caesium 132.9	56 Ba barium 137.3	57-71 lanthanoids	72 Hf hafnium 178.5	73 Ta tantalum 180.9	74 W tungsten 183.8	75 Re rhenium 186.2	76 Os osmium 190.2	77 Ir iridium 192.2	78 Pt platinum 195.1	79 Au gold 197.0	80 Hg mercury 200.6	81 Tl thallium [204.3, 204.4]	82 Pb lead 207.2	83 Bi bismuth 209.0	84 Po polonium	85 At astatine	86 Rn radon
87 Fr francium	88 Ra radium	89-103 actinoids	104 Rf rutherfordium	105 Db dubnium	106 Sg seaborgium	107 Bh bohrium	108 Hs hassium	109 Mt meitnerium	110 Ds darmstadtium	111 Rg roentgenium	112 Cn copernicium	113 Uut ununtrium	114 Fl flerovium	115 Uup ununpentium	116 Lv livermorium	117 Uus ununseptium	118 Uuo ununoctium

57 La lanthanum 138.9	58 Ce cerium 140.1	59 Pr praseodymium 140.9	60 Nd neodymium 144.2	61 Pm promethium	62 Sm samarium 150.4	63 Eu europium 152.0	64 Gd gadolinium 157.3	65 Tb terbium 158.9	66 Dy dysprosium 162.5	67 Ho holmium 164.9	68 Er erbium 167.3	69 Tm thulium 168.9	70 Yb ytterbium 173.0	71 Lu lutetium 175.0
89 Ac actinium	90 Th thorium 232.0	91 Pa protactinium 231.0	92 U uranium 238.0	93 Np neptunium	94 Pu plutonium	95 Am americium	96 Cm curium	97 Bk berkelium	98 Cf californium	99 Es einsteinium	100 Fm fermium	101 Md mendelevium	102 No nobelium	103 Lr lawrencium

INTERNATIONAL UNION OF PURE AND APPLIED CHEMISTRY

For notes and updates to this table, see www.iupac.org. This version is dated 8 January 2016.